Ln(III) complexes as potential phosphors for white LEDs

Akerboom, S.

1 Introduction

The anticipated growth of the world population and the increasing demand for energy are in stark contrast with the earth's energy resources that are rapidly nearing depletion. Substantial amounts of energy can be saved by employing more efficient sources of artificial light. Today's light sources are reviewed together with state-of-the-art solid state light sources (SSLs) that have great energy savings potential. Emphasis is put on the phosphors required for efficient SSLs and the potential of coordination compounds of trivalent lanthanoid ions as phosphors is discussed. The chapter is concluded with a description of the contents of this thesis.

1.1 Thirst for energy

1.1.1 Global energy consumption

Year after year, the world's energy consumption has been rising [1]. With the anticipated growth of the world population in mind it is to be expected that the thirst for energy will only increase further [1-3]. In 2011, the global use of primary energy was as high as 12,275 million tons of oil equivalent (Mtoe), or approximately 143 PWh [1]. Compared to the figure of 2001 (110 PWh) this is an increase of as much as 30% in 10 years. The consumption of primary energy by the 27 member states of the enlarged European Union (EU-27) was 13.5 PWh in 2007 [4, 5]. In principle, one can think of two possible ways of dealing with the growing thirst for energy. On the one hand, the production of energy can be increased accordingly. With most of our energy production relying on fossil fuels that are rapidly approaching depletion, this seems to be an inadequate response. On the other hand, the energy can be used more effectively, i.e. by employing more efficient technology. As will be discussed in the upcoming sections (1.2 and 1.3), there is a high savings potential when it comes to artificial lighting. Recent developments in the field of semiconductor technology have opened doors towards much more efficient light sources.

1.1.2 Electric energy consumption

In 2007, the total consumption of electric energy within the EU-27 was 2.9 PWh [4, 5]. Households were responsible for using 800.7 TWh of electric energy, while the tertiary sector consumed 760.4 TWh of electric energy. Approximately 10% (84 TWh) of the residential electricity consumption was due to electric lighting, while this figure is 26% (200 TWh) for the tertiary sector [4, 5]. Similar numbers are found for the consumption of electricity in the USA: it is estimated that 22% (915 TWh) of the electric energy produced is used for electric lighting [6]. These are rather substantial amounts of energy, so there is a high energy saving potential when it comes to electric lighting. Schubert *et al.* have estimated the energy savings potential provided by *solid state lighting* (SSL) (section 1.3.3) [6]. In their calculations, the SSL-lamps are assumed to be almost three times more efficient than the current ones, which is a realistic assumption as can be seen from Table 1.1. A 20% market penetration of SSL would lead to an annual saving of 230 TWh, which is 5.5% of the total US electricity production. An SSL penetration of 60% would lead to a saving of 459 TWh per year, or 11%. The impact on annual CO_2 emissions of the US for these scenarios is estimated to be 134 Mt and 268 Mt, respectively.

1.2 Lighting technology

1.2.1 General considerations

Currently, the most commonly used lamps for indoor lighting are based on relatively old technology and have been highly optimized in the past decades. Their efficiency has reached a limit that is inherent to their operating principles, leaving little possibilities for further improvement. SSL technology on the other hand is rapidly emerging, and has made extraordinary progress in the past decade. The efficiency of SSL-based lamps is now comparable to that of fluorescent technology, and there seems to be no fundamental reason why efficiencies could not increase even further [7].

1.2.2 Incandescent lamps and halogen lamps

The development of the incandescent lamp dates back to 1879, when Thomas Edison filed his patent on the 'Electric lamp' [8-10]. The principle of operation of the incandescent lamp relies on the thermal emission of radiation by a glowing tungsten wire. The wire, or *filament*, itself is heated by resistance heating, when a sufficiently large current passes through it to make it glow. As a result of this principle, the emission spectrum of an incandescent lamp very closely resembles that of a black body radiator and can be described by the Planck radiation formula [11, 12]. The emission spectrum is continuous and broad, with its maximum depending on the emission temperature according to Wien's law: $\lambda_{max} \times T = 2.897 \times 10^{-3}$ m · K [13, 14]. A major drawback of the black body emission is that a substantial amount of radiation is emitted in the infrared region. Integration of a 2,500 K black body emission spectrum shows that only 5% of the emission energy is within the visible region, the rest is lost as heat. Following Wien's law, the emission maximum may be shifted to shorter wavelengths by increasing the filament's temperature, but this approach is limited by the evaporation rate of tungsten, with its melting point at 3,695 K [15]. In the *halogen incandescent lamp*, the net rate of tungsten evaporation is reduced by employing a tungsten-halogen cycle.

Table 1.1: Characteristics of commercially available lamps.

Lamp	η_{eff} (lm · W^{-1})	CCT (K)	CRI
Incandescent	15 - 20	2800	100
Halogen incandescent	20 - 25	2800 - 3200	100
TL / CFL	30 - 100	2700 - 6500	50 - 95
White LED (typical)	80	6500	85
Warm-white LED	67	2700	> 70

η_{eff}: luminous efficacy, lumens per watt of electrical power drawn by the lamp. TL: 'Tube Luminescent' (French), CFL: Compact Fluorescent Lamp.

During operation of the lamp, tungsten will evaporate from the filament into the gas phase. There it will react with the halogen, typically iodine, to give a volatile tungsten halide. At the high operation temperatures, this halide will stay in the gas phase and decompose close to the filament, resulting in tungsten being deposited back on it [16]. This allows higher operating temperatures of the filament and thus increases light output. However, due to the broad nature of the emission spectrum, the efficiency increase is limited, as can be seen from Table 1.1.

1.2.3 Fluorescent lamps

Fluorescent lamps were introduced in 1938 by General Electric and compact fluorescent lamps (CFL's) were made available in the 1970s [17-19]. This type of lamps relies on a gas discharge of low pressure mercury vapor. The main emission of the mercury plasma is in the deep UV at 254 nm, which is not only invisible to the human eye but also harmful [11, 20, 21]. A coating of luminescent materials, often called *phosphors*, on the inside of the tube is used to convert this UV radiation into visible light. The overall energy conversion efficiency of fluorescent lamps is limited to about 30% [11, 22]. The main energy loss occurs in the conversion of deep UV photons to visible photons, which amounts to a loss of 50%. Further energy is lost in the plasma discharge process and in the conversion process by the phosphors. It is obvious that the majority of the losses are due to the operating principles of the lamp. Since the performance of the phosphors used currently is close to their physical limit, the efficiency of fluorescent lamps cannot be improved significantly [23].

1.2.4 Light-emitting diodes

As the name suggests, a light-emitting diode (LEDs) is a diode, which generally consists of a junction of n- and p-type semiconductors. A semiconductor can be described as a substance with a valence band that holds the valence electrons and an empty conduction band. The top of the valence band is separated from the bottom of the conduction band by the bandgap, which is characteristic for the compound. A semiconductor can be doped with atoms that have excess electrons compared to the host material (n-doping). This introduces an additional dopant level with electrons within the bandgap, close to the conduction band. Doping a semiconductor with an electron-poor atom introduces an empty band near the valence band of the semiconductor. When p- and n-type semiconductors are joined together, electrons from the n-type semiconductor flow to the p-type semiconductor, occupying the holes, until equilibrium is reached. Under the influence of an external electron motive force, electrons can be pumped from the valence band of the p-type semiconductor, to the higher energy conduction band of the n-type semiconductor. At the junction, the electrons and holes can recombine under the release of energy. In the case of a direct bandgap semiconductor, this energy can be released in the form of photons, that is,

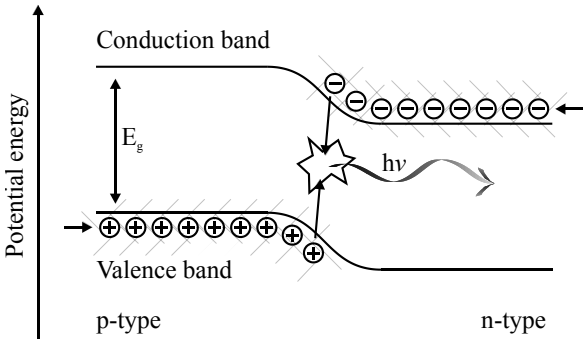

Figure 1.1: A PN-junction under forward bias, conducting a current and exhibiting luminescence as a result of radiative electron-hole recombination. E_g: bandgap, the current flows from the p-type to the n-type side of the junction.

light is emitted from the semiconductor. A schematic representation of this operating principle is given in Figure 1.1. This effect was discovered already in 1907 by H. J. Round, when testing SiC crystals as a rectifier for an early crystal-detector radio [12]. Thanks to this principle, electric energy is converted into light directly and in theory highly efficiently. Dependent on the intensity required by the application and the required color, several semiconductor systems are being used today, an overview is given in Table 1.2. Sustained development of LEDs based on GaAsP, GaP, GaAs and GaN was initiated in the 1960s. Most of the work on GaN technology was abandoned in the mid 1970s as a result of the poor efficiencies that were achieved by the early devices [12]. In 1992 however, Akasaki *et al.* demonstrated the first GaN LED emitting in the UV spectral region with a surprisingly high efficiency. From that moment on, development on GaN semiconductor technology has soared and LED technology can be used for producing all visible colors [24].

The green gap

The size of the bandgap is influenced by the dopants used in the semiconductor material and therefore dopant concentration can be used to tune the color of the light emitted by the

Table 1.2: Overview of the semiconductor systems used for commercial LEDs (source: [12]).

Semiconductor	Color	Brightness (rel.)
GaAsP:N	orange-red-IR	low
GaP:N	green	low
Al:GaAs	deep red-IR	high
$(Al_xGa_{1-x})_yIn_{1-y}P$	yellow-orange-red	high
In:GaN	nUV-blue-green	high

LED. For instance, pure GaN has a bandgap of 3.40 eV, corresponding to emission in the near-UV region at 365 nm [24]. This bandgap can be lowered by doping the material with indium, which allows the emission to shift to the blue and green spectral regions [25]. In theory, the In:GaN system could span the entire visible region, as the bandgap of pure InN is estimated to be between 0.7 and 0.8 eV, corresponding to emission in the IR region around 1600 cm^{-1} [26]. Doping the semiconductor has other effects. The $(Al_xGa_{1-x})_{0.5}In_{0.5}P$ system has a direct bandgap for $x < 0.5$ while a crossover to an indirect bandgap occurs for compositions with $x > 0.5$. The bandgap energy at the crossover point is 2.33 eV, which corresponds to 532 nm [12]. For the In:GaN system, the reasons for performance reduction at higher dopant concentrations are less well understood. It has been attributed to the immiscibility of GaN and InN and to increased strain between the In:GaN active layer and the GaN base layer [12, 27, 28]. So, while it is perfectly possible to prepare high efficiency blue and red LEDs based on GaN:In and $(Al_xGa_{1-x})_yIn_{1-y}P$, respectively, it has been proven impossible to obtain efficient green, yellow and amber LEDs. This problem is frequently referred to as the *green gap* or *yellow gap* [28, 29]. A plot of the external quantum efficiency *versus* the peak emission wavelength of commercially available LEDs is given in Figure 1.2. Also shown in this graph is the eye sensitivity curve (section 1.3.1). Since the eye is very sensitive in the region of the green gap, the inefficient LEDs still appear to exhibit bright emission.

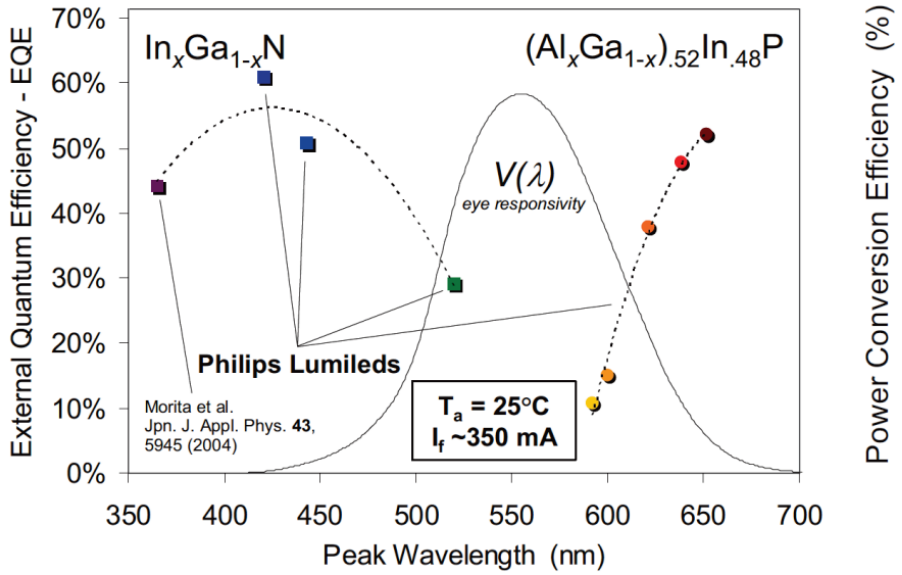

Figure 1.2: External quantum efficiency versus peak wavelength high power Philips Lumileds based on In:GaN (UV to blue region) and AlGaInP materials, superimposed on the eye sensitivity curve V(λ). The lack of high efficiency green and yellow LEDs is known as the 'green gap'. Image taken from ref. [27].

1.3 White light and light sources

1.3.1 White light

The human eye

The word *light* is used to indicate that part of the electromagnetic spectrum to which the human eye is sensitive. It is generally accepted that this part of the spectrum extends from 380 nm to 780 nm [30]. Before discussing the principles that the current light sources rely on to generate white light, it is fruitful to consider the characteristics of the human eye. In the eye, the lens focuses the light onto the retina, which contains light sensitive rod and cone cells. The rods are more sensitive to light than the cones and respond to the entire visible spectrum. They are useful in low-light conditions and do not allow color vision. The less sensitive cones require conditions of high ambient light, and there are three types of them, each of which is sensitive to a specific part of the visible spectrum, as shown in Figure 1.3. One can distinguish red-sensitive, green-sensitive and blue-sensitive cones based on their spectral response. Colors can be differentiated based on the relative stimulus of these three receptors [12, 30].

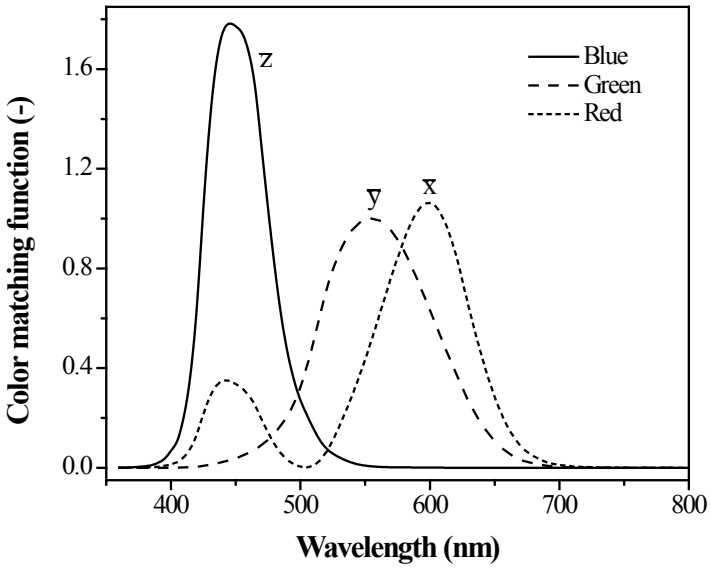

Figure 1.3: The sensitivity of the red, green and blue color receptors in the retina of the human eye. These curves are also known as the dimensionless color matching functions $\bar{x}(\lambda)$, $\bar{y}(\lambda)$ and $\bar{z}(\lambda)$. Note that $\bar{y}(\lambda)$ is equal to the eye-sensitiviy function V(λ). Redrawn using data taken from [12].

Colorimetry

The spectral response curves of the blue, red and green receptors in the eye shown in Figure 1.3 are also known as the *color matching functions* $\bar{x}(\lambda)$, $\bar{y}(\lambda)$ and $\bar{z}(\lambda)$, respectively [12, 30]. The *tristimulus values X*, *Y* and *Z* represent the degree of stimulation of each of the receptors by a light source with an emission spectrum *P(λ)* as shown in equation 1.

$$X = \int \bar{x}(\lambda) \cdot P(\lambda) d\lambda \qquad Y = \int \bar{y}(\lambda) \cdot P(\lambda) d\lambda \qquad Z = \int \bar{z}(\lambda) \cdot P(\lambda) d\lambda \qquad (1)$$

The total stimulus of the receptors in the eye is just $X + Y + Z$. This property allows for defining the ratios in equation 2, which represent the relative stimuli of the cones.

$$x = \frac{X}{X+Y+Z} \qquad y = \frac{Y}{X+Y+Z} \qquad z = \frac{Z}{X+Y+Z} \qquad (2)$$

As the value of z can be found from $z = 1 - x - y$, the z coordinate is redundant and x and y can be used to uniquely define a color in a two-dimensional color space, shown in Figure 1.4. The parameters x and y are the *chromaticity coordinates*. They can be used to locate all visible colors in the diagram; the lower left-hand corner corresponds to blue, the top to green and the right hand corner to red. As white light corresponds to equal stimulus of all three receptors, it is located in the center of the diagram.

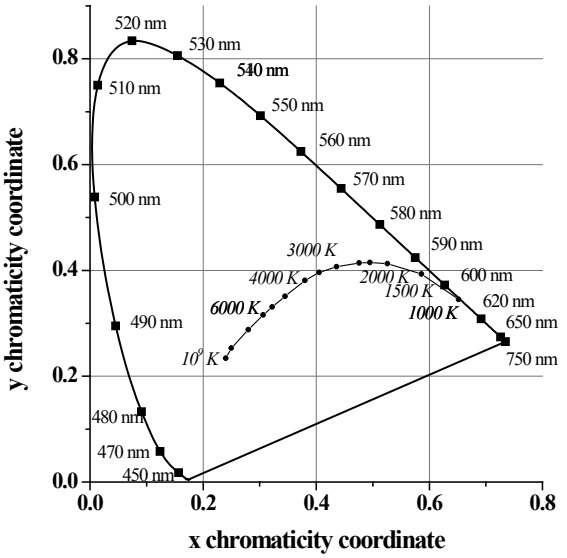

Figure 1.4: The Commission Internationale de l'Eclairage (CIE) 1931 color diagram showing the two-dimensional color space as defined by equation 2. Monochromatic colors are indicated on the perimeter of the diagram using squares. White light is located in the center at (0.33, 0.33) and the coordinates of black bodies in the temperature range from 1000 to 10^9 K are indicated by dots on the Planckian locus.

Characteristics of white light

A large number of possible optical spectra correspond to white light [12]. This is illustrated by the emission spectra shown in Figure 1.5a–e, all of which correspond to white light. Thus, a light source with a spectrum that contains only three narrow emission lines that match the maximum sensitivity of the three color receptors will be perceived as white. The same is true for a light source with an emission spectrum with a nearly constant intensity over the visible region. The difference between these two light sources can become apparent when they are used to illuminate an object. The observed color is a result of the interplay between the light source's emission spectrum and the object's light absorption spectrum. Therefore, the perceived color may differ between the two light sources. This phenomenon is described by the *color rendering index* (CRI) of the light source, which is defined as its ability to render a color with respect to a standard. The standard is usually daylight, and the CRI is specified on a scale from 0 (poor) to 100 (best). Another metric, the *correlated color temperature* (CCT), is used to indicate if a light source emits 'cold', bluish or 'warm' reddish white light. It is defined as the absolute temperature of an ideal black body emitter with its color coordinates as close as possible to that of the light source [12, 30]. For example, the CCT of a candle is somewhere between 1,500 and 2,000 K, that of an incandescent lamp 2,800 K and summer sunlight at noon between 4,900 and 5,700 K [12]. In Figure 1.4, the location of black body radiators is indicated by the *Planckian locus*. Interestingly, high color temperature light appears to be 'cold' because it is relatively rich in blue emission.

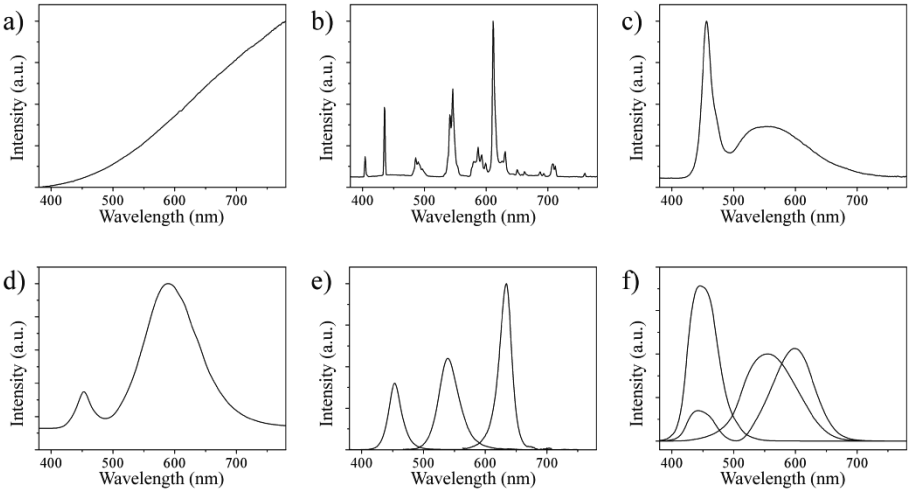

Figure 1.5: Emission spectra of a 40 W incandescent lamp (a), a typical TL lamp (b), a typical white LED (c), a warm white LED (d), a red, green and blue LED (e) and the sensitivity of the cones in the retina of the human eye (f).

Eye sensitivity

The characteristics of the eye also need to be considered when the energy performance of a lamp is measured. Although the total emitted power of radiation by a lamp is easily expressed as its *radiant flux* in units of Watts, this does not give information on the *perceived intensity*. For instance, the eye does not register the large amount of IR radiation emitted by an incandescent lamp; this is readily seen from Figure 1.5f. To take the eye sensitivity into account, *photometric units* are used. They describe the intensity of a light source as perceived by the eye. The result is expressed as *luminous efficiency* in lumens per Watt of optical power ($lm \cdot W^{-1}$). For a light source with an emission spectrum $P(\lambda)$, the luminous efficiency η_{lum} is given by equation 3 [12].

$$\eta_{lum} = 683 \frac{lm}{W} \cdot \int V(\lambda) P(\lambda) d\lambda \qquad (3)$$

In this equation, $V(\lambda)$ represents the *eye sensitivity function*, which is plotted in Figure 1.2. The maximum of the $V(\lambda)$ function is at 555 nm and the factor 683 has a historical origin [12]. The theoretical maximum luminous efficiency is thus 683 $lm \cdot W^{-1}$ for a monochromatic emitter at 555 nm. For efficient lamps and phosphor materials, a good match to the eye sensitivity function is an important prerequisite for obtaining high efficiency lighting. This is especially true for emitters in the red spectral region. The eye sensitivity falls off rapidly for wavelengths over 600 nm. For saturated red light, a red emitter with a λ_{max} of 610 nm is desired [7, 31]. This can be seen from Figure 1.4, where the lower right-hand corner corresponds to red. Use of a broad band emitter would result in substantial emission at wavelengths beyond 610 nm, reducing its luminous efficiency. Use of a line emitter that has otherwise the same λ_{max} and efficiency would reduce this spillover to longer wavelengths. As a result, the luminous efficiency of the light source has increased although the radiant flux remains unchanged. The overall efficiency of conversion of *electric power* into light by a lamp, also considering the sensitivity of the eye, is usually expressed as its *luminous efficacy*, also in $lm \cdot W^{-1}$ [12]. In this case, the Watts refer to the total electrical power drawn by the lamp.

1.3.2 Current lamps and white light

The spectrum of incandescent and halogen incandescent lamps is continuous over the entire visible region and extends deep into the infrared part. This ensures that all three receptors in the eye are stimulated, and since the spectrum is a Planck curve, the CRI of these light sources is high. In theory, a filament temperature of 6,620 K provides the best match to the human visual response and would give rise to a luminous efficiency of approximately 95 $lm \cdot W^{-1}$ [7]. The emission spectrum of fluorescent tubes strongly depends on the blend that has been applied on the inside of the tube. Typically, it consists of a mixture of phosphors with several emission lines or bands spread over the visible region, as is shown in Figure

1.5b. A comparison of characteristics of commercially available white lamps is given in Table 1.1 [9, 12, 32].

1.3.3 Solid-state lighting and white light

Although the conversion of electric energy into light can be accomplished with a high efficiency thanks to the semiconductor nature of LEDs, there is one important drawback: the emission is inherently monochromatic as it is determined by the size of the bandgap. Monochromatic light sources are useful for indicator lamps and traffic lights, but cannot be used to illuminate office-buildings and houses. Currently, several solutions to circumvent this drawback exist. The term *solid-state lighting* (SSL) is a collective expression for those LED-based white light sources.

RGB LEDs

Perhaps the most obvious solution to produce white light is to combine red, green and blue LEDs into a single device. Although this solution, also known as the *RGB LED*, has theoretically the highest efficiency, there are some downsides. The different LED chips are made using different semiconductor materials and will age at different rates, resulting in color instability of the emitted light [29]. Furthermore, the LEDs will require different driving voltages, which complicates the fabrication of an RGB LED [11, 33]. Finally, the efficiency of this solution is hampered by the comparatively low efficiency of green LED chips [29, 34]. This problem is discussed in section 1.2.4, and is inherent to the characteristics of the semiconductor materials used to produce LEDs [7, 29].

Blue LED with broadband phosphor

In an alternative approach for white light generation, a single LED chip is used to pump a layer of phosphor materials. White LEDs that rely on phosphor materials are commonly known as phosphor-converted white LEDs (PC-WLEDs). The most widely used white LEDs as of to date use an In:GaN LED emitting blue light at 470 nm combined with Ce:$Y_3Al_5O_{12}$, cerium-doped yttrium-aluminum garnet (Ce:YAG), as a phosphor material. When a current is passed through the LED, it starts emitting blue light, of which a fraction is absorbed to excite the phosphor material. The blue light of the LED, mixed with the broad band emission of the phosphor, results in white light. An emission spectrum of such device is shown in Figure 1.5c. Ever since the white LEDs of this type were commercialized in 1996, they have been applied in flashlights, bicycle lamps, car headlights and in other situations that do not require high quality white light [9, 12]. White LEDs of this type can achieve high luminous efficacies, but the lack of emission in the red spectral region generally results in high correlated color temperatures of over 6,500 K, making them unsuitable for general illumination purposes. More recently, so-called ‘warm white LEDs’ were made commercially available. The basic principle is similar: a blue LED, usually emitting at 450 nm, is used to pump a phosphor coating. The phosphor in this case

is usually a broad band emitting Eu(II)-doped $Ca_{m/2}Si_{12-m-n}Al_{m+n}O_nN_{16-n}$ (CaSiAlON) material [35, 36]. The emission from these white LEDs can achieve correlated color temperatures of 2700 K; the spectrum of such white LED is shown in Figure 1.5d. The CRI that is accomplished in this way is however limited to 70, which limits the applicability of these lamps [37-39]. In addition, degradation of the phosphor material or LED chip will cause significant color changes in time [33].

Near-UV LED with phosphor coating

An approach similar to the one taken for generating white light with fluorescent tubes is to use an LED emitting in the nUV region to pump a coating of blue, green and red phosphor materials [33, 40]. With this method it is possible to tune the color temperature and CRI just by changing the composition of the phosphor coating. At the same time, it requires driving only a single LED and provided that the phosphor materials are stable, color shifts are avoided over the entire lifespan of the LED. With this method, a high CRI as well as a high efficiency can be reached. It has been shown that a theoretical light source with three component colors can achieve a CRI of 85 at a luminous efficiency of 366 $lm \cdot W^{-1}$ [41]. Compared to the device based on a blue LED, the Stokes shift of the phosphor coating is larger when a nUV LED is used. However, this is compensated for by the higher efficiency of the nUV LED, as compared to the blue one. The effect of increasing efficiency of the In:GaN LEDs towards shorter wavelengths is illustrated by the dashed line in Figure 1.2.

1.4 Phosphor materials

1.4.1 General remarks on phosphor materials

The first phosphor material was discovered in the year 1603 by an Italian shoemaker and alchemist in Bologna, and is known as the *Bolognian stone* [42]. The material, $BaSO_4$ with traces of other elements, was found to absorb daylight and emit various colors in the dark. Other stones were found to exhibit similar behavior and these were named *phosphors*, meaning 'light bearer' in Greek. The name of the element *phosphorus* derives from the property of white phosphorus to show a faint glow when exposed to oxygen or air [42, 43]. As this glow is the result from the oxidation of phosphorus, the correct name for this process is *chemiluminescence*, not phosphorescence. Nowadays, although the meaning of *phosphor* is not clearly defined, the word generally refers to solid materials that exhibit *luminescence* [43]. Luminescence refers to the phenomenon in which a substance emits light after its electronic state has been excited by external energy. It includes both *phosphorescence* and *fluorescence*. The first refers to long afterglow phenomena linked to spin-forbidden electronic transitions, while the latter refers to extremely short afterglow associated with spin-allowed electronic transitions [13].

1.4.2 Current phosphors

Phosphor materials are widely applied in modern day technology such as luminescent tubes (*vide supra*), cathode ray tubes (CRT's) and plasma display panels (PDP's) [22, 32, 44]. These phosphors have been developed and optimized in the past several decades and have reached almost optimal photophysical properties, as strong absorption (> 90%) and high quantum efficiency (~90%). It can therefore not be expected that these properties can be significantly improved [22, 23]. Nearly all of these materials are based on inorganic compounds and are highly stable. They are, however, optimized for excitation with high energy photons. In a fluorescent lamp, a wavelength of 254 nm is used while in PDP's the phosphors are excited by vacuum UV (VUV) photons between 147 and 190 nm [11]. In CRT's, the excitation energy is even higher; a beam of high energy electrons (30 keV) is used [22]. While the current phosphors work well for those applications, they show poor absorption at 360–480 nm, limiting their usefulness for application in SSLs based on GaN LED technology.

1.4.3 Phosphors for PC-WLEDs

For the PC-WLED to become feasible, novel phosphor materials that can be excited by the LED chip are required [33, 45]. Besides Ce:YAG that is nowadays widely applied, other potential materials are investigated as phosphor for application in near-UV or blue LED based PC-WLEDs. In general, these materials comprise oxides, nitrides, oxynitrides, sulfides and silicates [33, 39, 40, 46]. Typically, most oxides show poor absorption in the nUV or blue region, while most sulfides are very sensitive to moisture and CO_2 [11, 33, 39]. Most of the oxide materials are garnet-type materials, but silicates, aluminates and borates are widely studied as well [33]. Oxynitrides and nitrides are investigated as host materials for Eu(II), as their strong crystal field results in a shift of the ion's emission into the red region. The resulting emission spectrum is of broadband nature, which is not desirable for a red phosphor. Beyond 610 nm, the sensitivity of the eye drops rapidly, as explained in section 1.3.1, so that emission at wavelengths over 610 nm contributes very little intensity. As a result, the lumen equivalent falls rapidly as the bandwidth of the red phosphor increases. The decrease in efficiency is roughly 0.15% per nanometer [7]. This can be compensated for by shifting the emission of the red phosphor to shorter wavelengths, but the lamp will not be able to render saturated red colors. To maintain a saturated red as well as a high efficiency, a narrowband phosphor emitting around 610 nm is highly desired [7]. Additional requirements, regardless of emission wavelength, arise from the very high photon flux of a typical high power LED. The excitation energy density generated by a 1 Watt In:GaN LED is estimated to be approximately 30 $W \cdot cm^{-2}$, which is nearly three orders of magnitude higher than the excitation energy density phosphors in a typical fluorescent tube are exposed to [11]. In addition, the temperature of high power LEDs can reach values of over 100 °C, because they are not perfectly efficient [47, 48].

To sum up, the perfect phosphor has [31, 49]:

1. An emission spectrum with high lumen equivalent
2. A high absorption in the n-UV to blue spectral region, matching In:GaN LEDs
3. A high quantum efficiency
4. High thermal- and photostability
5. Low thermal quenching

1.5 Trivalent lanthanoid ions

1.5.1 Lanthanoid ions and phosphor materials

The lanthanoid ions are widely used as emitting center in phosphor materials, because of their well defined and favorable photophysical properties (section 1.6). Most notable are the trivalent ions that show narrow, almost line-like emission bands that are relatively insensitive to the environment of the ion. As a result, they produce highly pure colors. The Eu(II) ion is used as emitting center in phosphors as well (*vide supra*), but it shows broad band emissions.

1.5.2 Nomenclature and discovery

When it comes to the nomenclature of the lanthanoids, there seems to be some disagreement. Although terms like *lanthanide*, *lanthanoid* and *rare earth* are loosely used, they are in fact well defined. According to the International Union of Pure and Applied Chemistry, the use of *lanthanide* should be avoided altogether as the ending '-ide' normally suggests a negative ion while the lanthanoids, being metals, only give rise to stable cations [50]. The term *lanthanoid*, meaning 'like lanthanum', is more correct and is a collective name for the elements La, Ce, Pr, Nd, Pm, Sm, Eu, Gd, Tb, Dy, Ho, Er, Tm, Yb, Lu. Although, given this definition, La should not be included in this series, it has become a member by common usage. The term 'lanthanoid' is derived from the Greek *lanthaneien*, meaning 'lying hidden' [51]. The *rare earths* encompass the lanthanoids together with Sc and Y [52]. The term 'rare earth' has an historical origin; 'earth' was commonly used to refer to oxide-type minerals in the 18th century. Earths containing the rare earth elements apparently seemed rare [53]. The history of rare earth chemistry starts in the late 18th century in Scandinavia, when Johan Gadolin discovers a new earth he names yttria. In the following years, more 'earths' were discovered, most of them consisting of a mixture of lanthanoid oxides. Successful separation into the constituent oxides was performed by Carl Gustav Mosander in the years 1839-1843. Lutetium was the last naturally-occurring rare earth to be discovered, by Urbain in 1907, while it took until 1947 to synthesize the artificial element promethium [53, 54]. It must be noted that these elements are in fact not as rare as the name suggests [53, 55, 56]. The terrestrial abundances range from 0.2 ppm for Tm to 46 ppm for Ce [56]. Thus, even the rarest rare earths are more abundant than gold (0.004 ppm), mercury (0.08 ppm) or Se (0.05 ppm) [57].

1.5.3 Mining, separation and chemical properties

Mining and separation

The lanthanoids are mainly found in nature in the minerals Bastnasite (LnFCO$_3$), Mozanite ((Ln,Th)PO$_4$) and Xenotime (Y,Ln)PO$_4$ [55, 56]. China has the world's largest lanthanoid reserve at approximately 60%, followed by the former Soviet Union at 17% and the United States at 13% [58]. The lanthanoids are extracted from the minerals by means of acid digestion, which results in the chloride salts, or by treatment with NaOH, producing lanthanoid hydroxides. Separation of the lanthanoid elements on a commercial scale is done by means of solvent extraction of lanthanoid nitrates between water and an organic solvent using tri-(*n*-butyl)phosphate as an extractant. Using repeated extractions can give the elements in a purity level of up to 99.99%, while ion-exchange methods are required to achieve purities of 99.999% [55, 56].

Basic chemical properties

Because the lanthanoids have highly similar chemical properties, it took over 100 years to completely separate them [53, 55]. They all have a stable +3 oxidation state, and the ionic radius changes smoothly from 1.06 Å for La(III) to 0.85 Å for Lu(III) [59]. The latter phenomenon is known as *lanthanoid contraction* and is tightly related to the properties of the 4f orbitals that, on going from La to Lu, are gradually filled with electrons. This 4f shell is located within the filled [Xe] core, so that the 4f orbitals are practically completely shielded from the environment by the filled 5s and 5p orbitals. In addition, the 4f electrons only partially compensate for the increase in nuclear charge, resulting in a net increase of the attractive force between the nucleus and the outer electrons and thus contraction [52]. This phenomenon is commonly known as *lanthanoid contraction*. In cases when a full ($4f^{14}$) or half full ($4f^{7}$) or empty ($4f^{0}$) shell can be achieved, additional oxidation states are possible. For this reason, Ce and Tb have a stable +4 oxidation state, while Eu and Yb can exist in a +2 oxidation state [52, 55]. The +3 oxidation state, which is common for all lanthanoids, is the result of optimal balance between ionization energy and the lattice or solvation energy [55, 60].

1.5.4 Coordination chemistry

The coordination chemistry of the lanthanoids was poorly investigated up until the mid 1960s. It was assumed that the lanthanoids would form 6-coordinate complexes, in analogy with the d-block elements [61]. However, much has been learned since. The coordination chemistry is largely governed by the +3 oxidation state, although complexes with for instance Eu(II) and Ce(IV) and Yb(II) have been reported [55, 62-64]. Owing to the properties of the shielded 4f valence electrons, the lanthanoids share many characteristics. They act as hard Lewis acids preferring hard Lewis bases such as O and F. Compared to the d-block metal ions, they all show a rather low coordination stabilization energy, and

complex formation as a result is mainly entropy-driven. Thus, polydentate ligands generally give rise to stable complexes. The stability of the bonds increases gradually on going from La(III) to Lu(III) as a result of the increased charge density on the smaller ions. Unlike d-block ions, the lanthanoid ions do not show a preferred coordination geometry and the bonding is mainly non-directional. The final geometry and coordination number are therefore mostly governed by the steric demands of the ligands. For example, spectroscopic evidence suggests that the early lanthanoids (La – Eu) form aqua complexes with a coordination number of 9, while the later ions (Dy – Lu) give rise to complexes described by $[Ln(H_2O)_8]^{3+}$ [55]. This is a direct result from lanthanoid contraction. Coordination numbers are reported to range from 2 to as high as 12 [60]. Care should be taken, though, because the coordination of the cyclopentadienyl ligand is often counted as 1 [52]. A coordination number of 8 is most commonly encountered for the lanthanoid ions. Lower coordination numbers can be achieved by increasing the steric bulk of the ligands, while higher numbers are accessible by using chelating ligands with a small coordination angle, such as the nitrate ion.

1.6 Photophysical properties of the trivalent lanthanoid ions

1.6.1 Electronic structure and energy levels

The interesting photophysical properties of the trivalent lanthanoid ions, such as the long luminescence lifetime and line-like emission spectra, are a direct result of the 4f orbitals being shielded by the 5s and 5p shells. The 4f orbitals are gradually filled on going from La(III) to Lu(III), and the electronic configuration changes from $[Xe]4f^0$ to $[Xe]4f^{14}$. Depending on the number of electrons, there are several ways to distribute them over the 4f orbitals. There are seven 4f orbitals, and each of them can hold two electrons, so there are a total of 14 positions or *spin-orbitals* available for the electrons to occupy. It can be shown that the number of possible arrangements (N) for distribution of n electrons over p orbitals is given by equation 4.

$$N = \frac{p!}{n!(p-n)!} \qquad (4)$$

The number of possible arrangements of the f electrons or *microstates*, for the trivalent lanthanoid ions is given in Table 1.3.

Table 1.3: Atomic number (Z), number of f-electrons and possible arrangements (N) and ground state energy term for the trivalent lanthanoid ions.

Ln(III)	Z	$4f^n$	N	Ground term
La	57	0	1	$^1S_0$
Ce	58	1	14	$^2F_{5/2}$
Pr	59	2	91	$^3H_4$
Nd	60	3	364	$^4I_{9/2}$
Pm	61	4	1001	$^5I_4$
Sm	62	5	2002	$^6H_{5/2}$
Eu	63	6	3003	$^7F_0$
Gd	64	7	3432	$^8S_{7/2}$
Tb	65	8	3003	$^7F_6$
Dy	66	9	2002	$^6H_{15/2}$
Ho	67	10	1001	$^5I_8$
Er	68	11	364	$^4I_{15/2}$
Tm	69	12	91	$^3H_6$
Yb	70	13	14	$^2F_{7/2}$
Lu	71	14	1	$^1S_0$

Spectroscopic terms and free-ion levels

Some electron arrangements will be more favorable than others as a result of a number of interactions that the electrons experience. By far the strongest interaction is the Coulomb repulsion between the electrons, resulting in splitting of the configuration into *spectroscopic terms*. The energy differences caused by this interaction are in the order of 10^4 cm^{-1} [65]. A spectroscopic term is characterized by the total orbital angular momentum (L) and total spin (S) corresponding to the distribution of the electrons. Following the Russel-Saunders coupling scheme, both L and S can be found from the orbital angular momentum (l) and spin (s) of the individual electrons by a vector sum, using equations 5 and 6.

$$\vec{L} = \vec{l}_1 + \vec{l}_2 + \cdots + \vec{l}_n \qquad (5)$$

$$\vec{S} = \vec{s}_1 + \vec{s}_2 + \cdots + \vec{s}_n \qquad (6)$$

A spectroscopic term has the general form $^{2S+1}\mathbf{L}$, with **L** depending on L according to Table 1.4, while the number $2S + 1$ indicates the spin multiplicity of the term.

Table 1.4: Term symbols corresponding to the first seven values of *L*.

L	0	1	2	3	4	5	6	7
L	S	P	D	F	G	H	I	K

Besides the Coulombic interaction that leads to splitting of a configuration into spectroscopic terms, there is a weaker interaction that splits the terms further into *levels*. It is the spin-orbit interaction, which results in energy differences in the order of 10^3 cm^{-1} [65]. The orbital and spin angular momenta of the electrons couple to give a total angular momentum *J*. For a given term, *J* can take values according to equation 7.

$$|\vec{L} - \vec{S}| \leq \vec{J} \leq |\vec{L} + \vec{S}| \qquad (7)$$

The number of levels within a given term is simply found from $(2L + 1) \times (2S + 1)$, and the levels are described by symbols of the general form $^{2S+1}\mathbf{L}_J$. These levels are the so-called free-ion energy levels, as up until here no influence of the environment has been taken into account. The symbol corresponding to the ground state level can be found using Hund's rules in the order given below [66].

1. The ground state level has the largest spin multiplicity
2. The ground state level has the highest orbital angular momentum
3. The *J*-value of the ground state of a $4f^n$ configuration is given by:
    - $J = |L - S|$ if $n \leq 6$
    - $J = S$ if $n = 7$
    - $J = |L + S|$ if $n \geq 8$

Crystal field splitting

When the lanthanoid ion is placed in a coordinating environment, a third and even weaker interaction must be taken into account. It is the electric field produced by the coordinating atoms, known as the crystal field, which results in splitting of the free-ion levels further into Stark levels. The energy differences caused by the crystal field are in the order of a few hundreds of cm^{-1} [65, 66]. The maximum number of Stark levels for each free ion level equals $(2J + 1)$, but the exact number depends on the geometry of the coordination sphere. As a result, the 4f – 4f transitions of the trivalent lanthanoids can be used to probe site symmetries, and the maximum number of Stark levels for a given site symmetry have been tabulated [66, 67]. The Stark levels are labeled using the symbols of the irreducible representations of the point group corresponding to the coordination polyhedron [65, 67]. Figure 1.6 schematically summarizes how the $4f^6$ configuration split up as a result from all interactions.

1.6.2 Radiative transitions and selection rules

Although the trivalent lanthanoids have numerous electronic microstates, as can be seen from Table 1.3, the number of possible transitions between them is restricted by selection rules. A photon can interact with the 4f electrons through its electric or magnetic component. Since a photon cannot change the spin of an electron, the spin selection rule

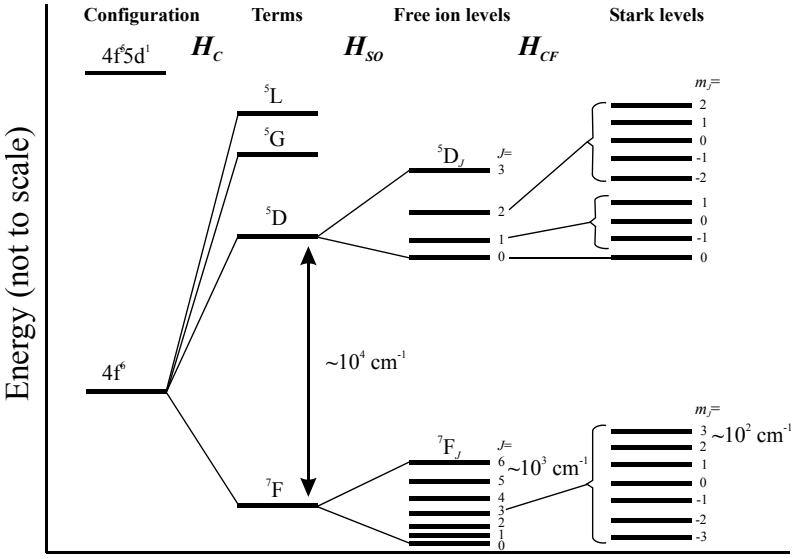

Figure 1.6: A schematic representation of the interactions that lead to splitting of the $4f^n$ configuration, here given (partially) for Eu^{3+}. From left to right: splitting due to Coulombic interactions (H_C), spin-orbit coupling (H_{SO}) and the crystal field (H_{CF}).

($\Delta S = 0$) easily follows. Interaction of the electron with the photon's electric-field component results in a net linear displacement of the electron. This phenomenon is known as an *electric dipole* (ED) transition, because there is dipole moment associated with this type of charge migration. Thus, transitions between s and p orbitals are allowed, because they involve a spatial redistribution of the charge, while transitions between s orbitals are forbidden. In the latter case, the charge shift has spherical symmetry and has no dipole moment associated. More formally, the ED operator has odd parity, the parity of the initial and final state of the electrons should be different. Hence, $4f^n \rightarrow 4f^n$ transitions are ED forbidden, as l for none of the electrons changes during such transition. The odd parity of the ED operator is illustrated schematically in Figure 1.7. The type of $4f^n - 4f^n$ transitions that are allowed are the *magnetic dipole* (MD) transitions. Interaction of the photon's magnetic-field component with the *trajectory* of the electron results in a rotational displacement of the entire trajectory. Transitions between s and p orbitals are MD forbidden, because this would involve a change in parity. A transition from a p_x orbital to a p_y orbital is MD allowed; a chemist will readily recognize that this can be seen as a rotation. Put more formally, the MD operator has even parity and it couples states of the same parity. Therefore it is the only type of allowed transition on an isolated *Ln*(III) ion. A pictorial representation of the effect of the MD operator and its even parity is given in Figure 1.7.

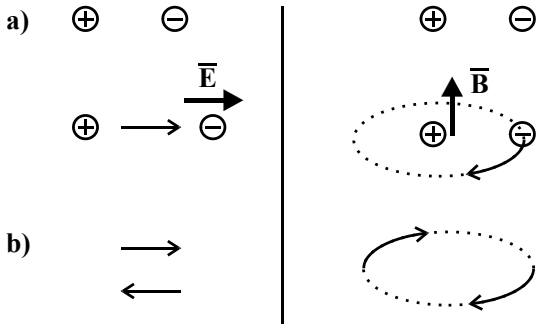

*Figure 1.7: a) A schematic representation of the effect of an ED (left) and MD (right) operator on an electron. The ED operator (thick arrow, **E**) results in a shift of the electron (thin arrow). The MD operator (thick arrow, **B**) results in shifting the electron over a circular trajectory. b) the effect of the inversion operation on the effect of the ED (left) and MD (right) operators. It can be seen that the effect of the ED operator changes sign, as the direction of the arrow is inversed. Thus, it has odd parity. For the MD operator, inversion does not invert the sense of rotation and so the MD operator has even parity.*

Lifting the selection rules: intermediate coupling

Following the above rules, only MD transitions would be allowed on an isolated lanthanoid ion. However, the large spin-orbit coupling constant of the heavy atomic nucleus of the lanthanoids also results in mixing of the free-ion levels for which $|\Delta L| = 1$ and $|\Delta S| = 1$ and $|\Delta J| = 0$. This phenomenon is known as *intermediate coupling* and as a result, L and S are only accurate quantum numbers to a certain extent. For instance, consider the $^5D_0 \rightarrow {}^7F_2$ transition of Eu(III), which is usually the strongest band in the emission spectrum. This spin forbidden transition should not occur according to the selection rules. The intermediate coupling scheme however enables a pathway for lifting the restrictions imposed by the parity and spin selection rules [68]. The $^5D_0$ level ($L = 2$, $S = 2$, $J = 0$) mixes with the $^7F_0$ level ($L = 3$, $S = 3$, $J = 0$) and the $^7F_2$ level ($L = 3$, $S = 3$, $J = 2$) mixes with the $^5D_2$ level ($L = 2$, $S = 2$, $J = 0$). Thus, although the $^5D_0$ level has still dominantly $^5D_0$ character, it also has some $^7F_0$ character, which helps alleviating the spin selection rule. The various types of transitions and the corresponding S, L, J selection rules are listed in Table 1.5.

Lifting the selection rules: crystal field

Another mechanism lifting the ED selection rule is the crystal field splitting, resulting from the electric field produced by the atoms surrounding the lanthanoid ion. If the crystal field symmetry is highly non-centrosymmetric, the crystal field helps mixing some opposite parity orbital character into the 4f orbitals. For example, some 5d character can be mixed into the 4f orbitals, similar to the formation of hybrid orbitals such as sp^3, sp^2 and sp on carbon atoms. As a result, the orbitals no longer are purely 4f-type, which enables a pathway for lifting the parity selection rule [68]. Transitions of this type are known as *forced ED* transitions, because they are 'forced' by the crystal field. Their intensity however is still only 10^{-4} times that of a fully allowed ED transition.

Table 1.5: Selection rules for several types of transitions and their properties [66, 68].

Type [a]	Parity	ΔS	ΔL	ΔJ	I_{rel} [b]
ED	Opposite	0	±1	0, ±1	1
Forced ED	Opposite	0	0, ±1, ±2, ±3, ±4, ±5, ±6; if L=0 or L'=0: ±2, ±4, ±6	0, ±1, ±2, ±3, ±4, ±5, ±6; if L=0 or L'=0: ±2, ±4, ±6	10^{-4}
MD	Same	0	0	0, ±1	10^{-6}
EQ	Same	0	0, ±1, ±2	0, ±1, ±2	10^{-10}

a) ED: Electric Dipole, MD: Magnetic Dipole, EQ: Electric Quadrupole. b) Typical intensity relative to a fully allowed ED transition.

Hypersensitivity

Because the 4f orbitals are shielded efficiently from the surroundings, the intensity of the majority of 4f – 4f transitions varies only within a factor of 2-3 in different host matrixes. However, the intensity of some transitions can increase by as much as a factor of 200 depending on the host environment of the ion [69, 70]. These so-called *hypersensitive transitions* obey the selection rules for electric quadrupole (EQ) transitions listed in Table 1.5, and are therefore also known as *pseudo-quadrupole* transitions [70]. An example of such transition is the $^5D_0 \rightarrow {}^7F_2$ transition on Eu(III). As of to date, there seems to be disagreement on whether the $^5D_4 \rightarrow {}^7F_6$ transition on Tb(III) exhibits hypersensitivity [69, 71].

1.6.3 Intensities of the transitions

Judd-Ofelt theory

A model for describing the intensities of the radiative 4f – 4f transitions of the lanthanoids has been developed independently by B.R. Judd and G.S. Ofelt in 1962 [72, 73]. This model is known as the *Judd-Ofelt theory* (JO theory), and it can be used to predict the intensity of a transition in absorption and emission spectra, the relative contribution of a transition to the luminescence spectrum and radiative lifetime of exited states [71, 74]. The model is semi-empirical and relies on only three parameters. In the JO theory, the dipole strength of a forced ED transition is expressed by equation 8.

$$D_{ED} = e^2 \sum_{\lambda=2,4,6} \Omega_\lambda |\langle J \left|\left| U^\lambda \right|\right| J' \rangle|^2 \qquad (8)$$

In equation 8, Ω_λ represents the JO-parameters that are dependent on the matrix surrounding the lanthanoid ion and the bracketed expressions are the squared reduced matrix elements of which the value is independent of the lanthanoid ion's host matrix. Furthermore, the matrix elements are dimensionless, and their values have been tabulated

[75]. In general, the rate A of a transition from an initial state of multiplicity J to a final state with multiplicity J' is given by equation 9.

$$A_{J-J'} = \frac{64\pi^4 \upsilon^3}{3h(2J+1)}\left[\frac{n(n^2+2)^2}{9} D_{ED} + n^3 D_{MD}\right] \quad (9)$$

In this equation, v represents the wavelength of the transition, J the multiplicity of the initial state, h Planck's constant and n the refractive index of the compound. The contributions of the electric and magnetic dipole strengths to the transition are indicated by D_{ED} and D_{MD}, respectively. The first can be calculated from equation 8, while MD components can be calculated and have been tabulated [71]. Typically, the calculations are performed in the centimeter-gram-second (cgs) system of units, using the appropriate values for h and e as listed in Table 1.6.

Table 1.6: conversion factors from cgs to SI and numerical values of useful constants [71].

Constant or unit	Value	Unit
h (Planck's constant)	$6.626 \cdot 10^{-27}$	erg · s
e (elementary charge)	$4.803 \cdot 10^{-10}$	esu
D_{MD} ($^5D_0 \rightarrow {}^7F_1$ on Eu(III))	$9.6 \cdot 10^{-42}$	$esu^2 \cdot cm^2$
esu (= 1 $erg^{1/2} \cdot cm^{1/2}$)	$3.336 \cdot 10^{-10}$	C
erg (= 1 $g \cdot cm^2 \cdot s^{-2}$)	$1 \cdot 10^{-7}$	J

JO theory applied to Eu(III) emission

A special case arises for Eu(III) emission spectra. Given the emission spectrum of an Eu(III) compound, calculation of the JO parameters is particularly straightforward. The transition from the $^5D_0$ resonance level to the $^7F_1$ level is purely of MD nature, while the $^5D_0 \rightarrow {}^7F_J$, $J = 2, 4, 6$ are purely of forced ED nature. Thus, based on equations 8 and 9, the theoretical intensities for those transitions are given by equations 10 and 11.

$$A_{0-1} = \frac{64\pi^4 \upsilon^3}{3h} n^3 D_{MD} \quad (10)$$

$$A_{0-2,4,6} = \frac{64\pi^4 \upsilon^3 e^2}{3h} \frac{n(n^2+2)^2}{9} \sum_{\lambda=2,4,6} \Omega_\lambda \left| \langle J \left| \left| U^\lambda \right| \right| J' \rangle \right|^2 \quad (11)$$

The remaining $^5D_0 \rightarrow {}^7F_J$, $J = 0, 3, 5$ transitions are forbidden in both ED and MD schemes and are not accounted for by JO-theory. In practice, these are indeed very weak. The squared reduced matrix elements required for evaluation of equation 11 can be found in literature and they are given in Table 1.7 [75, 76]. Since all non-diagonal matrix elements are zero, the sum in equation 11 reduces to a mere multiplication of the matrix element and the JO-parameter.

Table 1.7: Squared reduced matrix elements for analysis of the Eu(III) emission spectrum.

Transition	$\|\|U^{(2)}\|\|$	$\|\|U^{(4)}\|\|$	$\|\|U^{(6)}\|\|$
$^5D_0 \rightarrow {}^7F_2$	0.0032	0	0
$^5D_0 \rightarrow {}^7F_4$	0	0.0023	0
$^5D_0 \rightarrow {}^7F_6$	0	0	0.0002

The rate constant for the MD transition is readily calculated from equation 10, with D_{MD} given in Table 1.6, and equals approximately 49 s^{-1}. Provided that the spectrophotometer used to record the spectra has been corrected for the response of the detection system and calibrated to present the relative photon flow, experimental intensities can be found by integrating the corresponding lines in the spectrum [77]. The relative intensities of the $^5D_0 \rightarrow {}^7F_J$, $J = 0 - 6$ transitions with respect to the MD transition are easily found, and can be used to calculate the value of A_{0-6} using A_{0-1} as a yardstick. Summing these rates gives the total rate of radiative relaxation A_{rad} as shown in equation 12.

$$A_{rad} = \sum_J A_{0-J} \qquad (12)$$

1.6.4 Non-radiative relaxation

Decay of the excited state of the trivalent lanthanoid ions occurs not only *via* the radiative transitions described above; the energy can also be dissipated trough vibrations of the host lattice or complex in a process known as *multiphonon relaxation* [78]. The efficiency of this mode of relaxation depends on the size of the energy gap between the lowest lying excited state and the highest level of the ground state multiplet. A large gap requires more quanta to bridge it, making this mode of relaxation less favorable [51, 78]. A direct result of this *energy gap law* is the fact that *Ln*(III) luminescence occurs mostly from only one level, the *resonance level*, which is separated from the next lower lying level by a large energy gap. For Eu(III), this is the $^5D_0$ level, which is separated from the $^7F_6$ level by approximately 12,300 cm^{-1}, while for the Tb(III) ion the gap between the $^5D_4$ and $^7F_0$ levels is approximately 14,800 cm^{-1} [79]. Higher excited states such as $^5D_1$ and $^5D_2$ of Eu(III) are efficiently relaxed to the $^5D_0$ state by multiphonon relaxation, hence emission from these levels is rarely observed. It should be pointed out that certain selection rules apply to multiphonon relaxation processes, so the energy gap law cannot be used as an exclusive benchmark for judging the efficiency of multiphonon relaxation [80].

Intrinsic quantum yield

The lifetime of luminescence can be obtained experimentally (τ_{exp}); it contains contributions of both radiative and non radiative relaxation processes. With the rate of the radiative processes calculated using equation 12, the total rate of non-radiative relaxation processes can be calculated and expressed as A_{nrad}. Now, the total rate of depopulation of

the lanthanoid excited state, A_{tot}, can be expressed as $A_{tot} = A_{rad} + A_{nrad}$. The relation between τ_{exp} and A_{tot} is simply $A_{tot} = (\tau_{exp})^{-1}$, and equation 13 follows.

$$A_{tot} = \frac{1}{\tau_{exp}} = \frac{1}{\tau_{rad}} + \frac{1}{\tau_{nrad}} \quad (13)$$

The ratio between the rate of radiative relaxation and the total rate of relaxation is known as the *intrinsic quantum yield* Φ_{Ln} of the lanthanoid ion given by equation 14 [60, 81].

$$\Phi_{Ln} = \frac{A_{rad}}{A_{tot}} = \frac{\tau_{exp}}{\tau_{rad}} \quad (14)$$

1.7 Luminescent lanthanoid complexes

1.7.1 Historical notes

The study on luminescent lanthanoid complexes was initiated in 1942, when Weissman observed very intense luminescence characteristic for Eu(III) from crystals of europium salicylaldehyde when the compound was excited in the ligand-centered absorption band [82]. He realized that "excitation of the internal electronic system of the europium is provoked by light absorption in a region external to it". In 1957, Crosby observed similar behavior for an Yb(III) complex, and later also for complexes of Sm(III), Tb(III), Dy(III), Tm(III) and Yb(III) [83, 84]. In many cases, the luminescence that was observed upon ligand excitation was much brighter than that observed using direct excitation of the 4f manifold. The first extensive review on the subject was written by Crosby in 1966 [85]. In the early 1980s, research on luminescent lanthanoid complexes got a new impulse because it was realized that the compounds could be useful as medical imaging agent [86-88]. From that moment on, the photoluminescence of lanthanoid coordination compounds became a widely studied subject. The phenomenon of ligand-centered excitation of lanthanoid-centered luminescence became known as the *antenna effect* [88, 89].

1.7.2 Intramolecular energy transfer

Thanks to the ligand the lanthanoid center can be excited without having to rely on direct excitation using the forbidden 4f ← 4f transitions. The mechanism for this process is schematically shown in Figure 1.8 [51, 60, 90, 91]. It involves excitation of the ligand by means of an allowed transition. It is generally accepted that the ligand subsequently undergoes intersystem crossing (ISC) to an excited triplet state, followed by ligand-to-lanthanoid energy transfer. The lanthanoid ion will relax to its ground state as described in section 1.6, either radiatively or non-radiatively. At any stage of the transfer cascade, quenching may occur, reducing the luminescence efficiency. The overall quantum efficiency, Φ_{tot}, of this process is described by equation 15 [51, 60, 90].

$$\Phi_{tot} = \Phi_{ISC} \times \Phi_{ET} \times \Phi_{Ln} \quad (15)$$

In this equation, Φ_{ISC}, Φ_{ET} and Φ_{Ln}, represent the intersystem crossing, energy transfer and the lanthanoid ion's intrinsic quantum yields, respectively. The product of the first two is often referred to as the *sensitizer efficiency* $\eta_{sens} = \Phi_{ISC} \times \Phi_{ET}$, while Φ_{Ln} can be found from equation 14. Experimental evidence indicates that the energy transfer involves the triplet excited state of the ligand [83, 84, 88, 92, 93]. Although relaxation from the S* to the T* state of the ligand is spin-forbidden, the large spin-orbit coupling constant from the lanthanoid ion greatly aids in this process [51, 60, 91, 94]. Ligand to lanthanoid transfer directly from the singlet state cannot be ruled out completely, though, and has been reported [85, 88, 95, 96]. The ligand-centered energy levels in a lanthanoid complex can be determined by recording the absorption and emission spectrum for the Gd(III) analogs. As the first excited state of the Gd(III) ion, $^6P_{7/2}$ at 32,150 cm^{-1}, is generally much higher than the triplet state of a ligand, ET is not possible and the compound will exhibit ligand-centered phosphorescence from the T* state [60, 97-99].

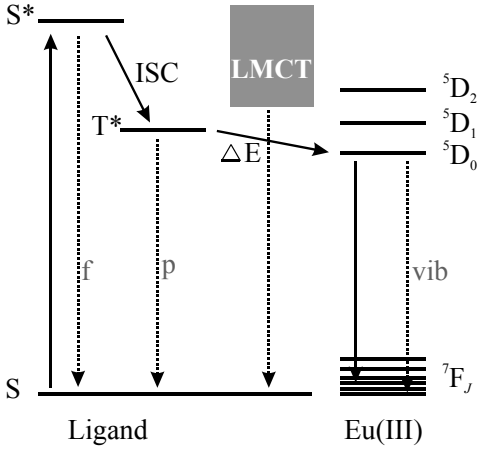

Figure 1.8: Jablonski diagram describing the energy transfer cascade in luminescent lanthanoid complexes. The preferred transfer pathway is indicated with uninterrupted arrows; quenching is indicated using dashed arrows. S/S: singlet ground- and excited state, T*: triplet excited state, ISC: intersystem crossing, LMCT: ligand-to-metal charge transfer band, ΔE: energy gap, f: fluorescence, p: phosphorescence, vib: vibrational quenching.*

Ligand to lanthanoid energy transfer

To describe energy transfer from the ligand to the lanthanoid ion, both Förster and Dexter type mechanisms can be invoked [51, 100-102]. Both transfer mechanisms are schematically shown in Figure 1.9. The Dexter mechanism involves a double electron transfer between the donor and acceptor and thus requires good overlap between the metal and ligand orbitals [103]. As a result, it is only efficient at very small distances between the ligand and the lanthanoid ion. In the Förster mechanism, the dipole moment of the ligand's excited state couples with that of the lanthanoid 4f levels [104]. For efficient Förster

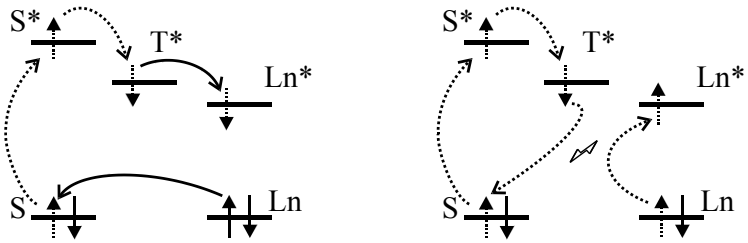

Figure 1.9: Schematic representation of Dexter (left) and Förster energy transfer mechanisms between the ligand and the lanthanoid ion. Transfer of electrons between the ligand and lanthanoid ion are indicated by solid arrows, dotted arrows indicate electronic processes within the ligand or lanthanoid ion.

transfer, large oscillator strengths are required. The group of Malta has derived a set of selection rules for Förster and Dexter type energy transfer mechanisms in luminescent lanthanoid complexes [97, 102]. Soon after the discovery of the antenna effect, it was realized that the level of the ligand-centered excited state with respect to the lanthanoid-centered resonance level plays an important role in the energy transfer process [84]. Systematic studies have shown that the energy gap between the T* state and the accepting level of the lanthanoid ion should be less than 1,850 cm^{-1} for efficient transfer [93]. That is, there should be a match between the ligand donor level and lanthanoid acceptor level. This match can be expressed as the *spectral overlap* in the Förster and Dexter transfer mechanisms [103-105]. If the gap is too small, thermally-assisted energy back-transfer may take place, providing a way of quenching the lanthanoid luminescence [51, 60, 86]. Another quenching pathway occurs in complexes based on lanthanoid ions having a low reduction potential, such as Eu(III) and Yb(III) (see 1.5.3) combined with a ligand that is easily oxidized [88]. In these compounds, ligand-to-metal charge transfer (LMCT) states may occur at levels sufficiently low to allow competition with L* → *Ln* energy transfer and thus cause quenching [51, 98, 106-108]. A theoretical framework describing energy transfer processes and the role of the LMCT state has been developed by Malta and co-workers [102, 106, 109-111].

Lanthanoid luminescence and quenching

Provided that the lanthanoid excited state is fed by the ligands, the complex should exhibit luminescence typical for the lanthanoid ion. As discussed in section 1.6.4, luminescence may be quenched by multiphonon quenching. In lanthanoid complexes, these phonons exist as high energy vibrational modes of C–H, O–H and N–H bonds [54, 86, 112]. As a rule of thumb, multiphonon relaxation is efficient if ΔE of the energy gap between two lanthanoid centered levels is equal to or smaller than six vibrational quanta [54, 113]. Considering C–H and O–H vibrations in the ligand, at 2,950 and 3,450 cm^{-1} respectively, it follows that these are efficient quenchers of Eu(III) and Tb(III) centered luminescence. Indeed, it is

known that water molecules in the first coordination sphere of Eu(III) are highly efficient luminescence quenchers. As the vibrational relaxation competes with the radiative route, its effectiveness may be assessed by recording the luminescence lifetime of the compound [112-114]. A suggested way of suppressing this mode of quenching is to replace the C–H and O–H bonds by C–D (ν = 2,100 cm^{-1}), C–F (ν = 1,200 cm^{-1}) and O–D (ν = 2,500 cm^{-1}) bonds [86, 115]. Meshkova *et al*. have demonstrated that substitution of the central C–H by a C–D bond in the β-diketone type ligand of a luminescent Yb(III) complex leads to an increase of the luminescence lifetime by 10 to 20% [112].

1.7.3 Examples of luminescent lanthanoid complexes

Several approaches have been taken to develop lanthanoid complexes showing highly efficient luminescence, and several reviews have been devoted to this subject in the past two decades [51, 60, 81, 86, 91, 97, 108, 115, 116]. The number of (potential) applications is large; besides use as phosphor materials (section 1.7.4) luminescent lanthanoid complexes can be used as, for example, imaging agents, biomarkers, immunoassays, pH sensors and O_2 sensors [81, 108, 117-119]. Suitable antenna ligands have hard donor atoms, and often have conjugated or aromatic systems to allow efficient light absorption at the desired wavelengths.

Complexes with β-diketonates

The β-diketonates constitute a very important class of ligands for luminescent complexes; the frequently used structures are shown in Figure 1.10. Several β-diketonates were used in the early studies by Weissman and have been the subject of several studies devoted to unraveling the energy transfer mechanism [82, 120-122]. Also in more recent studies β-diketonates continue to be used as ligands, and an extensive review on this class of compounds has been written by Binnemans [123]. Three β-diketonate ligands in their deprotonated form are required to counterbalance the positive charge on the lanthanoid ions. The coordination sphere is not saturated in such compounds, and solvent molecules will coordinate to the lanthanoid ion. To prevent this, a second ligand can be added to the reaction mixture to expel water and reduce quenching. If the ligand has an aromatic system, such as 1,10-phenanthroline, it may even act as an antenna. Examples of frequently used secondary ligands are shown in Figure 1.11. Homoleptic *tetrakis*-diketonato complexes can be prepared by employing a 1:4 metal-to-ligand ratio during synthesis. Depending on the synthetic strategy, the necessary cation can be provided by protonation of the base, e.g. the use of triethylamine gives $HNEt_3[EuL_4]$, or by using NaOH to deprotonate the β-diketone and addition of a chloride salt of the cation, such as NEt_4Cl [123, 124]. Alternatively, a quaternary ammonium hydroxide may be used as a base and source of the cation [125]. Other examples of counter ions used include the tetraphenylphosphonium, tetraphenylarsonium, 1,3-disubstitited imidazolium, morpholinium and

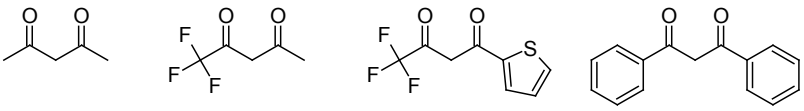

Figure 1.10: Examples of some widely used β-diketone ligands. From left to right: acetyl acetone (Hacac), trifluoroacetyl acetone (Htfac), 2-thenoyltrifluoroacetone (Httfa),dibenzoylmethane (Hdbm).

N-methylpyridinium ions [123, 124, 126-129].The β-diketonate ligands are highly efficient at sensitizing luminescence of the Eu(III) ion, because the triplet states closely match the ion's resonance level [97]. At approximately 21,000 cm^{-1}, the triplet state is too low for efficient population the $^5D_4$ level of the Tb(III) ion so that luminescence is rarely observed for Tb-dbm complexes, although exceptions have been reported [130]. Substituents on the ligand allow for tuning it to the metal, and can have a profound impact on its antenna properties [120]. In case of the tetrakis complexes, it was found that the cation provides additional handlebars for changing the luminescent properties of a given complex [124]. The highest luminescence quantum efficiency reported for a luminescent Eu(III) complex in the solid state is 85% for $[Eu(ttfa)_3(dbso)_2]$, (ttfa = trifluoroacetylacetonate; dbso = dibenzylsulfoxide) reported by Malta *et al.* [131]. For comparison, the quantum yield of $[Eu(ttfa)_3(H_2O)_2]$ is found to be only 23%, illustrating efficient quenching by the water molecules [132]. Very high photoluminescence quantum yields have also been reported for $HNEt_3[Eu(dbm)_4]$ at 75% [133]. Highly luminescent europium complexes can be obtained using this class of ligands; the compounds are however prone to photobleaching under UV radiation [123]. For example, Malta *et al.* have studied the temporal photoluminescence intensity of $[Eu(tta)_3(dbso)_2]$, and found that after 50 hours of irradiation at 400 nm, the luminescence intensity had dropped to 30% of its initial value [134].

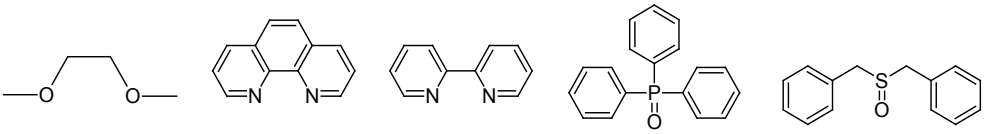

Figure 1.11:Examples of frequently used secondary ligands in lanthanoid(III) tris(dbm) complexes. From left to right: 1,2-dimethoxyethane (monoglyme), 1,10-phenanthroline (phen), 2,2'-bipyridine (bpy), triphenylphosphineoxide (tppo), dibenzylsulfoxide (dbso).

Small aromatic ligands

Many different and relatively small aromatic polydentate ligands can be successfully used to give photoluminescent lanthanoid complexes. For example, picolinates, salicylates, aromatic carboxylates and derived molecules have been used. Examples of such ligands are given in Figure 1.12. As with the β-diketonates, multiple ligands are required to saturate the coordination sphere around the central ion. Highly stable lanthanoid complexes showing very bright luminescence have been reported. For example, $[Eu(pbca)_3]$ (pbca = 4-phenyl-2,2'-bipyridine-5-carboxylate) has a luminescence quantum yield of 60%, while this figure for $[Tb(pbca)_3]$ is only 7% [135]. The complex $[Eu(bpc)_3]\cdot CH_3CN$ (bpc =

6-(1*H*-benzimidazol-2-yl)pyridine-2-carboxylate) is again very efficient at 61% quantum efficiency [136]. 2,6-Dipicolinic acid (H_2dpa) efficiently sensitizes both Eu(III) and Tb(III) centered luminescence, with quantum efficiencies of 72% and 68%, respectively [137]. Long luminescence lifetimes have been reported for complexes with the related amide ligand 2,6-pyridine-dicarboxamide (H_2pcam), shown in Figure 1.12b: 1.9 ms for $[Eu(pcam)_3](CF_3SO_3)_3$ and 2.2 ms for its Tb(III) analog [138]. While Eu(III) salicylates are often found to exhibit weak photoluminescence due to the presence of a low-lying LMCT state, the dinitro-substituted ligand (Figure 1.12c) is found to give Eu(III) complexes exhibiting very bright photoluminescence. This effect is explained by the increase of the energy of the LMCT state by the electron-withdrawing nitro group [139, 140].

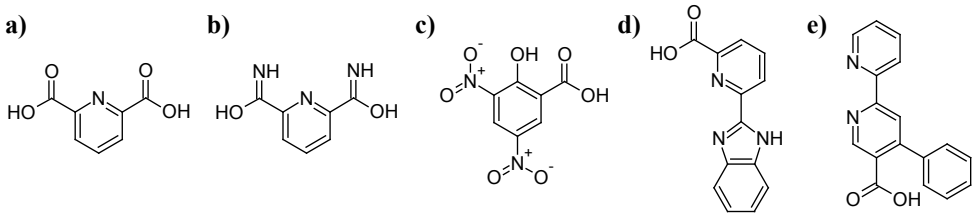

Figure 1.12: Overview of small aromatic ligands used in luminescent lanthanoid complexes. Shown are (a) 2,6-dipicolinic acid, H_2dpa, (b) 2,6-pyridine-dicarboxamide, H_2pcam, (c) 3,5-dinitrosalicylic acid, $H_2$3,5-NO_2-sal, (d) 6-(1H-benzimidazol-2-yl)pyridine-2-carboxylic acid, Hbpc, and (e) 4-phenyl-2,2'-bipyridine-5-carboxylic acid, Hpbca [135-138, 140-142].

Molecular cages

As complex formation is mostly entropy driven for lanthanoid ions, a successful strategy towards a stable complex is to use polydentate ligands that are able to fully encapsulate the lanthanoid ion. For luminescent complexes, one may distinguish ligands with chromophoric chelates and ligands with pendant chromophores [100]. The first have the antenna-part coordinating directly to the lanthanoid ion, while the latter have an antenna part that does not necessarily coordinate to the ion directly. Instead, the chromophore is attached to a ligand such as 1,4,7,10-tetraazacyclododecane (cyclen) (Figure 1.13b and c) or 1,4,7-triaza-cyclononane (TACN). When the antenna-part of the ligand is unable to coordinate to the lanthanoid ion, as for the ligand shown in Figure 1.13c, energy transfer is only possible via the through-space Förster-type mechanism [100, 104]. Ligands of the chromophoric chelate type bind to the lanthanoid ion through atoms that are part of the chromophore (Figure 1.13a, d and e) and allow both Förster and Dexter type energy transfer mechanisms [100, 103, 104]. Both the pendant chromophore and the chromophoric chelate approach towards cage-type ligands have led to lanthanoid complexes showing efficient photoluminescence. For example, the ligand in Figure 1.13d gives rise to Eu(III) and Tb(III) compounds that exhibit quantum yields in D_2O of 20% and 35%, respectively [89]. The ligand shown in Figure 1.13e forms a Tb(III) complex with a photoluminescence quantum yield of 61% in H_2O, while the analogous Eu(III) complex only manages to reach 6% [143].

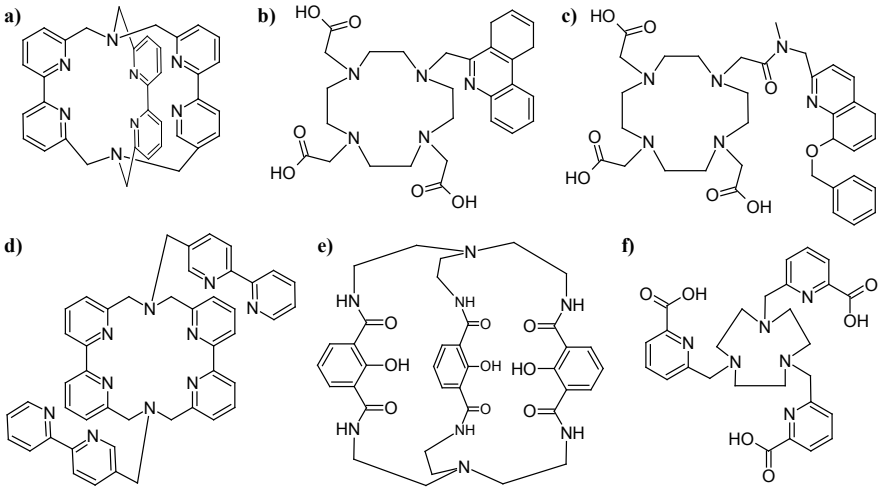

Figure 1.13: Examples of cage-type ligands used for photoluminescent Eu(III) and Tb(III) complexes. Ligands a, b, d and e and f belong to the chromophoric chelates category, while ligand c is an example of an antenna ligand with a pendant chromophore [89, 98, 143-146].

Metal organic frameworks

Thus far only isolated, mononuclear complexes have been considered. It is however perfectly possible to synthesize luminescent *metal organic frameworks*, or MOFs, using the lanthanoid ions. Typically, the ligands contain several groups that allow them to form bridges between the metal centers, thus forming an extended network of interlinked complexes. An overview of ligands that have been used in the preparation of photoluminescent lanthanoid(III) based MOFs is given in Figure 1.14. Synthesis of these compounds is usually performed under solvothermal conditions, that is, the reaction mixture is heated well above the solvent's boiling point in a pressure vessel. Alternative pathways, however, relying on a microwave or a carefully chosen mixture of solvents at room temperature have been reported [147-149]. An interesting feature of MOFs is demonstrated by Kerbellec and co-workers. They have reported luminescence for both $[Eu_2(bdc)_3]_n$ and $[Tb_2(bdc)_3]_n$ (bdc = 1,4-benzenedicarboxylate) with quantum efficiencies of 12% and 26%, respectively [150]. More recently, they found that it is possible to use a mixture of Eu(III) and Tb(III) ions in the reaction mixture, which allowed them to change the emission color from green to red by varying x in $[(Eu_{2-x}Tb_x)(bdc)_3]_n$ [151]. Inclusion of other metal ions such as Ca(II) and Na(I) to provide additional cross-links within the structure has proven to be successful, too [152, 153].

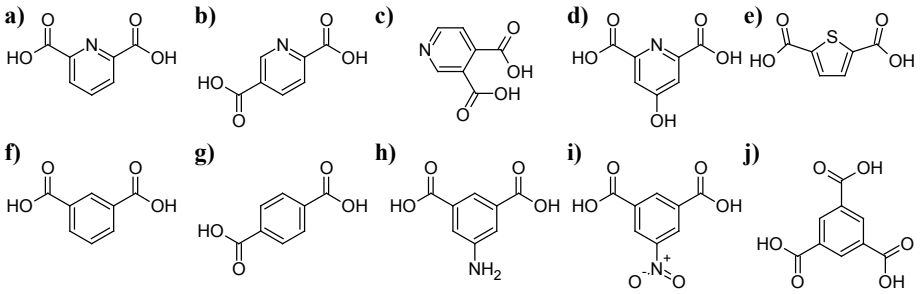

Figure 1.14: Overview of ligands that have been used for preparing MOFs with Ln(III) ions. (a) 2,6-dipicolinic acid, 2,6-H_2dpa, (b)2,5-H_2dpa, (c) 3,4-H_2dpa, (d) 4-hydroxylpyridine-2,6-dicarboxylic acid, H_3pdc, (e) thiophene-2,5-dicarboxylic acid, H_2tbc, (f)1,3-isophthalic acid, 1,3-H_2ipa, (g) 1,4-benzenedicarboxylic acid, H_2bdc, (h) 5-NH_2-1,3H_2ipa, (i) 5-NO_2-1,3H_2ipa, (j) 1,3,5-benzenetricarboxylic acid, H_3btc [149-152, 154-162].

1.7.4 Lanthanoid complexes as phosphor materials

The requirements for LED-phosphors listed in section 1.4.3 must be met before application in commercial LEDs can be considered. The use of europium(III) complexes as actual phosphors in LEDs has been demonstrated recently [163-166]. The complexes used are all of the β-diketonate type, and show quantum efficiencies ranging from 16% to 34% and in each case an LED emitting at 395 nm was used. Most of these investigations concern a single phosphor converted red In:GaN-based LED. Wang and co-workers have prepared a white LED using a europium complex as a red phosphor together with $BaMgA_{l1}O_{17}$:Eu(II) as a blue and ZnS:Cu(I):Al(III) as a green phosphor [166]. Still, the quantum yields of the complexes used were relatively low, and need to be improved. In addition, long term stability of the complexes must be ensured. The β-diketonate complexes are known to be prone to photobleaching, which may severely reduce the lifetime of the final SSL device [123, 134, 167].

Comparison with solid state phosphors

The phosphor materials that are widely used as of to date are typically based on inorganic oxides. As discussed in section 1.4.2, these materials are highly efficient and stable. However, they cannot be efficiently excited in the nUV range. Present research on developing new solid state phosphors appears to focus on Eu(II) based compounds [40, 41]. The emission color of these compounds is governed by the crystal field splitting of the excited $4f^6 5d^1$ configuration of the ion's excited state. While the broad band emission of the Eu(II) ion is not problematic for blue and green emitting phosphors, it is a problem for the red phosphor as deep-red emission contributes very little to the perceived light output (sections 1.3.1 and 1.4.3). Owing to its sharp emission line at 614 nm, the Eu(III) ion is a suitable emitter for creating an efficient phosphor. Recent investigations on suitable host materials for the Eu(III) ion focus on the use of molybdates and tungstates and are aimed at

shifting the lattice absorption into the nUV region. Generally, these compounds are claimed to be efficient red phosphors for nUV LEDs [168-171]. This is a doubtful statement, because excitation in the nUV region relies on the 4f ← 4f transitions on the Eu(III) ion centered at 395 nm [172]. Although these transitions usually appear to be strong in the excitation spectra, they are in fact weak due to their forbidden nature (section 1.6). This is illustrated by the diffuse reflectance spectra for $LiEu(WO_4)_{2-x}(MoO_4)_x$, in which the 4f – 4f transitions are weak compared to the allowed charge transfer band, although they are very intense in the excitation spectrum [171]. Other major drawbacks, making oxide type materials relatively expensive, are the synthesis temperatures and the required purity of the starting compounds. A typical synthesis of Ce:YAG involves temperatures in excess of 1500 °C [33]. High purity starting compounds (> 4N) are needed to avoid luminescence-quenching defects in the final phosphor material. For example, the photoluminescence quantum yield of Y_2O_3:Eu is reduced by as much as 7% in the presence of only 5 ppm Fe^{3+} impurity [20, 173]. Finally, a cost-effective method for recovery of the lanthanoids from oxides is still to be found [174-177]. Recycling of the lanthanoids has recently become attractive as China, which presently produces over 90% of all rare earths, has tightened its export quota [58, 176, 178]. Lanthanoid complexes are the class of compounds that can overcome these problems. Synthesis is typically performed at relatively low temperatures (< 200 °C) and owing to the molecular nature of lanthanoid complexes, there is no need for highly pure reactants. Both properties can substantially reduce production costs. In addition, the lanthanoids can be recovered by simply burning off the ligands. The absorption properties can be tuned to match the excitation source by making small modifications to the ligand, for instance by introducing substituents, while the favorable luminescent properties of the lanthanoid ion are retained. The main shortcomings that must be overcome before application of lanthanoid complexes as a phosphor material can be considered are the typically low quantum efficiency and poor long-term stability [123, 134, 165, 179, 180]. As described in section 1.7.3, exceptions to these general notions have been reported, justifying further research on the use of lanthanoid complexes as phosphor materials in LEDs.

1.8 Aim and scope of this thesis

Despite the many efforts to red-shift the excitation band of oxide-based phosphor materials to the nUV spectral region to allow for application in PC-WLEDs, no suitable material has been identified. The aim of the work described in this thesis is to synthesize complexes of Eu(III) and Tb(III) ions with ligands capable of efficient sensitization of luminescence of those ions upon excitation in the nUV region. In the present chapter, an introduction into the subject is given, as well as a description of the problems. In Chapter 2, the synthesis of derivatives of 1,10-phenanthroline as ligands to Eu(III), and the photophysical properties of the complexes with these ligands are described. In Chapter 3, the synthesis and photoluminescent properties of Eu(III) and Tb(III) compounds with novel small aromatic

ligands, giving rise to metal-organic frameworks (MOFs), are discussed. Another class of complexes using small ligands is discussed in Chapter 4, where phenol-type molecules are used to sensitize both Eu(III) and Tb(III) luminescence. In Chapter 5, the photoluminescence of Eu(III)-complexes with several substituted dibenzoylmethanates is discussed, and the influence of the counter ions is demonstrated. Chapter 6 concerns the photo and triboluminescent properties of the series $HNEt_3[Eu(dbm)_4]$. Chapter 7 contains a summary of this work, some concluding remarks and the future prospects. Appendix A deals with some details on photoluminescence quantum yield determinations.

Parts of this thesis are submitted for publication [181-185] or are in preparation.

1.9 References

[1] BP, *BP Statistical Review of World Energy*, 2012, Available from: www.bp.com/statisticalreview

[2] D. Pimentel, *Environ. Dev. Sustain.*, 14 (2012) 151-152.

[3] C. Pasten and J.C. Santamarina, *Energ. Policy*, 49 (2012) 468-476.

[4] P. Bertoldi and B. Atanasiu, *Electricity consumption and efficiëncy trends in the enlarged European union status report 2009*, 2009, Available from: http://iet.jrc.ec.europa.eu/energyefficiency/publication/electricity-consumption-and-efficiency-trends-european-union-status-report-2009

[5] B. Atanasiu and P. Bertoldi, *Int. J. Green Energy*, 7 (2010) 552-575.

[6] E.F. Schubert, J.K. Kim, H. Luo, and J.Q. Xi, *Rep. Prog. Phys.*, 69 (2006) 3069-3099.

[7] J.M. Phillips, M.E. Coltrin, M.H. Crawford, A.J. Fischer, M.R. Krames, R. Mueller-Mach, G.O. Mueller, Y. Ohno, L.E.S. Rohwer, J.A. Simmons, and J.Y. Tsao, *Laser Photonics Rev.*, 1 (2007) 307-333.

[8] E.F. Schubert and J.K. Kim, *Science*, 308 (2005) 1274-1278.

[9] Y. Narukawa, M. Ichikawa, D. Sanga, M. Sano, and T. Mukai, *J. Phys. D: Appl. Phys.*, 43 (2010) 354002.

[10] T.A. Edison, Electric lamp, Pat.no US223898, 1879.

[11] C.R. Ronda, *Luminescence - From Theory to Applications*, 2008: Wiley-VCH Verlag GmbH, Weinheim.

[12] E.F. Schubert, *Light-Emitting Diodes, 2nd edition*, 2006: Cambridge University Press, New York.

[13] P.W. Atkins and J. de Paula, *Atkins' Physical Chemistry, 8th edition*, 2006: W.H. Freeman and Company, New York.

[14] M. Csele, *Fundamentals of Light Souces and Lasers*, 2004: John Wiley & Sons, Hoboken, NJ, USA.

[15] *CRC Handbook of Chemistry and Physics, 85th edition*, 2005: CRC Press, Boca Raton.

[16] G.M. Neumann, *Thermochim. Acta*, 8 (1974) 369-379.

[17] F. Meyer, H.J. Spanner, and E. Germer, Metal vapor lamp, Pat.no US2182732, 1939.

[18] J.M. Anderson, Short arc fluorescent lamp, Pat.no US4093893, 1978.

[19] W.J. Roche, Single-base, self-igniting fluorescent lamp, Pat.no US3849699, 1974.

[20] G. Blasse and B.C. Grabmaier, *Luminescent Materials*, 1994: Springer Verlag, Berlin.
[21] R.N. Thayer and B.T. Barnes, *J. Opt. Soc. Am.*, 29 (1939) 131-134.
[22] T. Justel, H. Nikol, and C. Ronda, *Angew. Chem., Int. Ed.*, 37 (1998) 3085-3103.
[23] G. Blasse, *J. Alloy. Compd.*, 225 (1995) 529-533.
[24] F.A. Ponce and D.P. Bour, *Nature*, 386 (1997) 351-359.
[25] S. Nakamura, T. Mukai, and M. Senoh, *Appl. Phys. Lett.*, 64 (1994) 1687-1689.
[26] J. Wu, W. Walukiewicz, K.M. Yu, J.W. Ager III, E.E. Haller, H. Lu, W.J. Schaff, Y. Saito, and Y. Nanishi, *Appl. Phys. Lett.*, 80 (2002) 3967-3969.
[27] G. Chen, M. Craven, A. Kim, A. Munkholm, S. Watanabe, M. Camras, W. Götz, and F. Steranka, *Phys. Status Solidi A*, 205 (2008) 1086-1092.
[28] R. Mueller-Mach, G.O. Mueller, M.R. Krames, O.B. Shchekin, P.J. Schmidt, H. Bechtel, C.-H. Chen, and O. Steigelmann, *Phys. Status Solidi RRL*, 3 (2009) 215-217.
[29] J.R. Oh, S.-H. Cho, J.H. Oh, Y.-K. Kim, Y.-H. Lee, W. Kim, and Y.R. Do, *Opt. Express*, 19 (2011) 4188-4198.
[30] N. Kohei and K. Sueko, *Color vision*, in *Phosphor Handbook*, 2006, CRC Press, Boca Raton.
[31] L.E. Shea-Rohwer, J.E. Martin, X. Cai, and D.F. Kelley, *J. Solid State Sci. Technol.*, 2 (2013) R3112-R3118.
[32] C.R. Ronda, T. Justel, and H. Nikol, *J. Alloy. Compd.*, 277 (1998) 669-676.
[33] S. Ye, F. Xiao, Y.X. Pan, Y.Y. Ma, and Q.Y. Zhang, *Mater. Sci. Eng., R*, 71 (2010) 1-34.
[34] J.H. Oh, S.J. Yang, Y.-G. Sung, and Y.R. Do, *Opt. Express*, 20 (2012) 20276-20285.
[35] M. Raukas, J. Kelso, Y. Zheng, K. Bergenek, D. Eisert, A. Linkov, and F. Jermann, *J. Solid State Sci. Technol.*, 2 (2013) R3168-R3176.
[36] R.-J. Xie, N. Hirosaki, T. Takeda, and T. Suehiro, *J. Solid State Sci. Technol.*, 2 (2013) R3031-R3040.
[37] R.-J. Xie, N. Hirosaki, M. Mitomo, K. Sakuma, and N. Kimura, *Appl. Phys. Lett.*, 89 (2006) 241103.
[38] R.-J. Xie, N. Hirosaki, M. Mitomo, K. Takahashi, and K. Sakuma, *Appl. Phys. Lett.*, 88 (2006) 101104.
[39] R.-J. Xie and N. Hirosaki, *Sci. Technol. Adv. Mat.*, 8 (2007) 588-600.
[40] C.C. Lin and R.-S. Liu, *J. Phys. Chem. Lett.*, 2 (2011) 1268-1277.
[41] A. Zukauskas, R. Vaicekauskas, F. Ivanauskas, R. Gaska, and M.S. Shur, *Appl. Phys. Lett.*, 80 (2002) 234-236.
[42] E.N. Harvey, *A History of Luminescence*, 1957: American Philosophical Society, Philidelphia.
[43] S. Shigeo, *Introduction to the handbook*, in *Phosphor Handbook*, 2006, CRC Press, Boca Raton.
[44] C.R. Ronda, *J. Alloy. Compd.*, 225 (1995) 534-538.
[45] H.A. Höppe, *Angew. Chem., Int. Ed.*, 48 (2009) 3572-3582.
[46] R.-J. Xie, N. Hirosaki, N. Kimura, K. Sakuma, and M. Mitomo, *Appl. Phys. Lett.*, 90 (2007) 191101.
[47] K. Dowling, *Phys. Today*, 61 (2008) 74-75.
[48] U. Lafont, H. van Zeijl, and S. van der Zwaag, *Microelectron. Reliab.*, 52 (2012) 71-89.

[49] J. McKittrick, M.E. Hannah, A. Piquette, J.K. Han, J.I. Choi, M. Anc, M. Galvez, H. Lugauer, J.B. Talbot, and K.C. Mishra, *J. Solid State Sci. Technol.*, 2 (2013) R3119-R3131.
[50] N.G. Connelly, R.M. Hartshorn, T. Damhus, and A.T. Hutton, *Nomenclature of Inorganic-Chemistry (the Red Book) - IUPAC Recommendations*, 2005: Cambridge.
[51] J.-C.G. Bünzli and C. Piguet, *Chem. Soc. Rev.*, 34 (2005) 1048-1077.
[52] C. Huang, *Rare Earth Coordination Chemistry*, 2010: John Wiley & Sons, Singapore.
[53] F. Szabadvary, *The history of the discovery and separation of the rare earths*, in *Handbook on the Physics and Chemistry of Rare Earths*, 1988, Elsevier. 33-80.
[54] J.-C.G. Bünzli, S. Comby, A.-S. Chauvin, and C.D.B. Vandevyver, *J. Rare Earth.*, 25 (2007) 257-274.
[55] S. Cotton, *Lanthanide and Actinide Chemistry*, 2006: John Wiley & Sons, Chichester, UK.
[56] V.S. Sastri, J.-C.G. Bünzli, V. Ramachandra Rao, G.V.S. Rayudu, and J.R. Perumareddi, *Modern Aspects of Rare Earths and their Complexes*, 2003: Elsevier.
[57] S.R. Taylor, *Geochim. Cosmochim. Acta*, 28 (1964) 1273-1285.
[58] S. Massari and M. Ruberti, *Resour. Policy*, 38 (2013) 36-43.
[59] W.-K. Li, G.-d. Zhou, and T.C.W. Mak, *Advanced structural inorganic chemistry*, 2008: Oxford University Press, New York.
[60] L. Armelao, S. Quici, F. Barigelletti, G. Accorsi, G. Bottaro, M. Cavazzini, and E. Tondello, *Coord. Chem. Rev.*, 254 (2010) 487-505.
[61] R.E. Whan and G.A. Crosby, *J. Mol. Spectrosc.*, 8 (1962) 315-327.
[62] G.-Y. Adachi, K. Sorita, K. Kawata, K. Tomokiyo, and J. Shiokawa, *J. Less-common. Met.*, 93 (1983) 81-87.
[63] Y. Yao, Y. Zhang, Z. Zhang, Q. Shen, and K. Yu, *Organometallics*, 22 (2003) 2876-2882.
[64] J. Garcia and M.J. Allen, *Eur. J. Inorg. Chem.*, 2012 (2012) 4550-4563.
[65] B.M. Walsh, *Judd-Ofelt theory: principles and practices*, in *Advances in Spectroscopy for Lasers and Sensing*, 2006, Springer Netherlands. 403-433.
[66] J.-C.G. Bünzli and S.V. Eliseeva, *Basics of Lanthanide Photophysics*, in *Lanthanide Luminescence*, 2011, Springer Berlin Heidelberg. 1-45.
[67] C. Görller-Walrand and K. Binnemans, *Rationalization of crystal field parametrization*, in *Handbook on the physics and chemistry of the rare earths*, 1996, Elsevier. 121-284.
[68] P.A. Tanner and C.-K. Duan, *Coord. Chem. Rev.*, 254 (2010) 3026-3029.
[69] G. Ligner, R. Mohan, S. Knittel, and G. Duportail, *Spectrochim. Acta A*, 46 (1990) 797-802.
[70] C.K. Jørgensen and B.R. Judd, *Mol. Phys.*, 8 (1964) 281-290.
[71] C. Görller-Walrand and K. Binnemans, *Spectral intensities of f-f transitions*, in *Handbook on the Physics and Chemistry of Rare Earths*, 1998, Elsevier. 99-264.
[72] B.R. Judd, *Phys. Rev.*, 127 (1962) 750-761.
[73] G.S. Ofelt, *J. Chem. Phys.*, 37 (1962) 511-520.
[74] M.P. Hehlen, M.G. Brik, and K.W. Krämer, *J. Lumin.*, 136 (2013) 221-239.
[75] M.H.V. Werts, R.T.F. Jukes, and J.W. Verhoeven, *Phys. Chem. Chem. Phys.*, 4 (2002) 1542-1548.

[76] R. Reisfeld, E. Zigansky, and M. Gaft, *Mol. Phys.*, 102 (2004) 1319 - 1330.
[77] J.W. Verhoeven, *Pure Appl. Chem.*, 68 (1996) 2223-2286.
[78] M.H.V. Werts, *Sci. Prog.*, 88 (2005) 101-131.
[79] W.T. Carnall, P.R. Fields, and K. Rajnak, *J. Chem. Phys.*, 49 (1968) 4450-4455.
[80] M.J. Weber, *Phys. Rev. B*, 8 (1973) 54-64.
[81] J.-C.G. Bünzli, *Chem. Rev.*, 110 (2010) 2729-2755.
[82] S.I. Weissman, *J. Chem. Phys.*, 10 (1942) 214-217.
[83] G.A. Crosby and M. Kasha, *Spectrochim. Acta*, 10 (1958) 377-382.
[84] G.A. Crosby, R.E. Whan, and R.M. Alire, *J. Chem. Phys.*, 34 (1961) 743-748.
[85] G.A. Crosby, *Mol. Cryst.*, 1 (1966) 37-81.
[86] Y. Hasegawa, Y. Wada, and S. Yanagida, *J. Photochem. Photobiol., C*, 5 (2004) 183-202.
[87] H. Takalo, I. Hemmilä, T. Sutela, and M. Latva, *Helv. Chim. Acta*, 79 (1996) 789-802.
[88] G.E. Buono-core, H. Li, and B. Marciniak, *Coord. Chem. Rev.*, 99 (1990) 55-87.
[89] B. Alpha, R. Ballardini, V. Balzani, J.-M. Lehn, S. Perathoner, and N. Sabbatini, *Photochem. Photobiol.*, 52 (1990) 299-306.
[90] F. Gutierrez, C. Tedeschi, L. Maron, J.-P. Daudey, R. Poteau, J. Azema, P. Tisnès, and C. Picard, *Dalton Trans.*, (2004) 1334 -1347.
[91] K. Binnemans, *Chem. Rev.*, 109 (2009) 4283-4374.
[92] J.J. Freeman and G.A. Crosby, *J. Phys. Chem.*, 67 (1963) 2717-2723.
[93] M. Latva, H. Takalo, V.M. Mukkala, C. Matachescu, J.C. Rodriguez-Ubis, and J. Kankare, *J. Lumin.*, 75 (1997) 149-169.
[94] G.A. Hebbink, L. Grave, L.A. Woldering, D.N. Reinhoudt, and F.C.J.M. van Veggel, *J. Phys. Chem. A*, 107 (2003) 2483-2491.
[95] G.A. Hebbink, S.I. Klink, L. Grave, P.G.B.O. Alink, and F.C.J.M. van Veggel, *ChemPhysChem*, 3 (2002) 1014-1018.
[96] J.R.G. Thorne, J.M. Rey, R.G. Denning, S.E. Watkins, M. Etchells, M. Green, and V. Christou, *J. Phys. Chem. A*, 106 (2002) 4014-4021.
[97] G.F. de Sa, O.L. Malta, C.D. Donega, A.M. Simas, R.L. Longo, P.A. Santa-Cruz, and E.F. da Silva, *Coord. Chem. Rev.*, 196 (2000) 165-195.
[98] L. Prodi, M. Maestri, R. Ziessel, and V. Balzani, *Inorg. Chem.*, 30 (1991) 3798-3802.
[99] W.T. Carnall, P.R. Fields, and K. Rajnak, *J. Chem. Phys.*, 49 (1968) 4443-4446.
[100] E.G. Moore, A.P.S. Samuel, and K.N. Raymond, *Acc. Chem. Res.*, 42 (2009) 542-552.
[101] B. Yan, H. Zhang, S. Wang, and J. Ni, *J. Photochem. Photobiol., A*, 116 (1998) 209-214.
[102] F.R. Gonçalves e Silva, O.L. Malta, C. Reinhard, H.-U. Güdel, C. Piguet, J.E. Moser, and J.-C.G. Bünzli, *The Journal of Physical Chemistry A*, 106 (2002) 1670-1677.
[103] D.L. Dexter, *J. Chem. Phys.*, 21 (1953) 836-850.
[104] T. Förster, *Chem. Phys. Lett.*, 12 (1971) 422-424.
[105] L. Smentek and A. Kedziorski, *J. Lumin.*, 130 (2010) 1154-1159.
[106] W.M. Faustino, O.L. Malta, and G.F. de Sa, *J. Chem. Phys.*, 122 (2005) 054109.
[107] S. Petoud, J.-C.G. Bünzli, T. Glanzman, C. Piguet, Q. Xiang, and R.P. Thummel, *J. Lumin.*, 82 (1999) 69-79.

[108] N. Sabbatini, M. Guardigli, and J.M. Lehn, *Coord. Chem. Rev.*, 123 (1993) 201-228.
[109] F.R.G. e Silva and O.L. Malta, *J. Alloy. Compd.*, 250 (1997) 427-430.
[110] O.L. Malta, *J. Lumin.*, 71 (1997) 229-236.
[111] O.L. Malta and F.R. Gonçalves e Silva, *Spectrochim. Acta A*, 54 (1998) 1593-1599.
[112] S. Meshkova, Z. Topilova, M. Lozinskii, and D. Bol'shoi, *J. Appl. Spectrosc.*, 64 (1997) 229-233.
[113] G. Stein and E. Würzberg, *J. Chem. Phys.*, 62 (1975) 208-213.
[114] G.R. Choppin and D.R. Peterman, *Coord. Chem. Rev.*, 174 (1998) 283-299.
[115] S. Yanagida, Y. Hasegawa, K. Murakoshi, Y. Wada, N. Nakashima, and T. Yamanaka, *Coord. Chem. Rev.*, 171 (1998) 461-480.
[116] S. Faulkner, S.J.A. Pope, and B.P. Burton-Pye, *Appl. Spectrosc. Rev.*, 40 (2005) 1-31.
[117] D. Parker, P.K. Senanayake, and J.A.G. Williams, *J. Chem. Soc., Perkin Trans. 2*, (1998) 2129-2140.
[118] E. Pershagen, J. Nordholm, and K.E. Borbas, *J. Am. Chem. Soc.*, 134 (2012) 9832-9835.
[119] I. Hemmilä, *J. Alloy. Compd.*, 225 (1995) 480-485.
[120] N. Filipescu, W.F. Sager, and F.A. Serafin, *J. Phys. Chem.*, 68 (1964) 3324-3346.
[121] W.F. Sager, N. Filipescu, and F.A. Serafin, *J. Phys. Chem.*, 69 (1965) 1092-1100.
[122] L.R. Melby and N.J. Rose, Eight coordinate trivalent rare earth metal chelates with β-diketones, Pat.no US 3254103, 1966.
[123] K. Binnemans, *Rare earth beta-diketonates*, in *Handbook on the Physics and Chemistry of Rare Earths*, 2005, Elsevier. 107-272.
[124] A. Mech, M. Karbowiak, C. Görller-Walrand, and R. Van Deun, *J. Alloy. Compd.*, 451 (2008) 215-219.
[125] H. Bauer, J. Blanc, and D.L. Ross, *J. Am. Chem. Soc.*, 86 (1964) 5125-5131.
[126] X.-F. Chen, X.-H. Zhu, W. Chen, J.J. Vittal, G.-K. Tan, J. Wu, and X.-Z. You, *J. Coord. Chem.*, 52 (2000) 97-110.
[127] K. Goossens, P. Nockemann, K. Driesen, B. Goderis, C. Görller-Walrand, K. Van Hecke, L. Van Meervelt, E. Pouzet, K. Binnemans, and T. Cardinaels, *Chem. Mater.*, 20 (2007) 157-168.
[128] K. Lunstroot, K. Driesen, P. Nockemann, K. Van Hecke, L. Van Meervelt, C. Gorller-Walrand, K. Binnemans, S. Bellayer, L. Viau, J. Le Bideau, and A. Vioux, *Dalton Trans.*, (2009) 298-306.
[129] X.-R. Zeng, R.-G. Xiong, X.-Z. You, and K.-K. Cheung, *Inorg. Chem. Commun.*, 3 (2000) 341-344.
[130] H. Jiu, G. Liu, Z. Zhang, Y. Fu, J. Chen, T. Fan, and L. Zhang, *J. Rare Earth.*, 29 (2011) 741-745.
[131] O.L. Malta, H.F. Brito, J.F.S. Menezes, F.R. Gonçalves e Silva, C. de Mello Donegá, and S. Alves, *Chem. Phys. Lett.*, 282 (1998) 233-238.
[132] F.R.G. e Silva, J.F.S. Menezes, G.B. Rocha, S. Alves, H.F. Brito, R.L. Longo, and O.L. Malta, *J. Alloy. Compd.*, 303-304 (2000) 364-370.
[133] G. Bourhill, L.O. Pålsson, I.D.W. Samuel, I.C. Sage, I.D.H. Oswald, and J.P. Duignan, *Chem. Phys. Lett.*, 336 (2001) 234-241.
[134] L.D. Carlos, C.D.M. Donegá, R.Q. Albuquerque, S. Alves, J.F.S. Menezes, and O.L. Malta, *Mol. Phys.*, 101 (2003) 1037 - 1045.

[135] G.S. Kottas, M. Mehlstäubl, R. Fröhlich, and L. De Cola, *Eur. J. Inorg. Chem.*, 2007 (2007) 3465-3468.
[136] N.M. Shavaleev, S.V. Eliseeva, R. Scopelliti, and J.-C.G. Bünzli, *Chem.-Eur. J.*, 15 (2009) 10790-10802.
[137] T.J. Mooibroek, P. Gamez, A. Pevec, M. Kasunič, B. Kozlevčar, W.T. Fu, and J. Reedijk, *Dalton Trans.*, 39 (2010) 6483-6487.
[138] S. Tanase, P.M. Gallego, R. de Gelder, and W.T. Fu, *Inorg. Chim. Acta*, 360 (2007) 102-108.
[139] V. Tsaryuk, K. Zhuravlev, V. Zolin, P. Gawryszewska, J. Legendziewicz, V. Kudryashova, and I. Pekareva, *J. Photochem. Photobiol., A*, 177 (2006) 314-323.
[140] V. Tsaryuk, K. Zhuravlev, V. Kudryashova, V. Zolin, Y. Yakovlev, and J. Legendziewicz, *Spectrochim. Acta A*, 72 (2009) 1020-1025.
[141] K. Zhuravlev, V. Tsaryuk, J. Legendziewicz, V. Kudryashova, P. Gawryszewska, and V. Zolin, *Opt. Mater.*, 31 (2009) 1822-1824.
[142] P.A. Brayshaw, J.-C.G. Bünzli, P. Froidevaux, J.M. Harrowfield, Y. Kim, and A.N. Sobolev, *Inorg. Chem.*, 34 (1995) 2068-2076.
[143] S. Petoud, S.M. Cohen, J.-C.G. Bünzli, and K.N. Raymond, *J. Am. Chem. Soc.*, 125 (2003) 13324-13325.
[144] J.P. Cross, A. Dadabhoy, and P.G. Sammes, *J. Lumin.*, 110 (2004) 113-124.
[145] D. Maffeo and J.A.G. Williams, *Inorg. Chim. Acta*, 355 (2003) 127-136.
[146] J.W. Walton, R. Carr, N.H. Evans, A.M. Funk, A.M. Kenwright, D. Parker, D.S. Yufit, M. Botta, S. De Pinto, and K.L. Wong, *Inorg. Chem.*, 51 (2012) 8042-8056.
[147] N. Stock and S. Biswas, *Chem. Rev.*, 112 (2011) 933-969.
[148] Z.-J. Lin, Z. Yang, T.-F. Liu, Y.-B. Huang, and R. Cao, *Inorg. Chem.*, 51 (2012) 1813-1820.
[149] S.-P. Chen, Y.-X. Ren, W.-T. Wang, and S.-L. Gao, *Dalton Trans.*, 39 (2010) 1552-1557.
[150] C. Daiguebonne, N. Kerbellec, O. Guillou, J.-C.G. Bünzli, F. Gumy, L. Catala, T. Mallah, N. Audebrand, Y. Gérault, K. Bernot, and G. Calvez, *Inorg. Chem.*, 47 (2008) 3700-3708.
[151] N. Kerbellec, D. Kustaryono, V. Haquin, M. Etienne, C. Daiguebonne, and O. Guillou, *Inorg. Chem.*, 48 (2009) 2837-2843.
[152] M. Li, L. Yuan, H. Li, and J. Sun, *Inorg. Chem. Commun.*, 10 (2007) 1281-1284.
[153] T. Zhu, K. Ikarashi, T. Ishigaki, K. Uematsu, K. Toda, H. Okawa, and M. Sato, *Inorg. Chim. Acta*, 362 (2009) 3407-3414.
[154] C. Qin, X.-L. Wang, E.-B. Wang, and Z.-M. Su, *Inorg. Chem.*, 44 (2005) 7122-7129.
[155] Y.-g. Huang, B.-l. Wu, D.-q. Yuan, Y.-q. Xu, F.-l. Jiang, and M.-c. Hong, *Inorg. Chem.*, 46 (2007) 1171-1176.
[156] H.-H. Song and Y.-J. Li, *Inorg. Chim. Acta*, 361 (2008) 1421-1425.
[157] K. Liu, G. Jia, Y. Zheng, Y. Song, M. Yang, Y. Huang, L. Zhang, and H. You, *Inorg. Chem. Commun.*, 12 (2009) 1246-1249.
[158] D.-Y. Ma, H.-P. Zeng, Y.-W. Li, and J. Li, *Solid State Sci.*, 11 (2009) 1065-1070.
[159] X.-Q. Zhao, B. Zhao, S. Wei, and P. Cheng, *Inorg. Chem.*, 48 (2009) 11048-11057.
[160] F. Pellé, P. Aschehoug, S. Surblé, F. Millange, C. Serre, and G. Férey, *J. Solid State Chem.*, 183 (2010) 795-802.

[161] C.-H. Zhan, F. Wang, Y. Kang, and J. Zhang, *Inorg. Chem.*, 51 (2011) 523-530.
[162] X. Zhao, D.-X. Wang, Q. Chen, J.-B. Chen, G.-Y. Lin, S.-T. Yue, and Y.-P. Cai, *Inorg. Chem. Commun.*, 23 (2012) 127-131.
[163] G. Shao, Y. Li, K. Feng, F. Gan, and M. Gong, *Sens. Actuators, B*, 173 (2012) 692-697.
[164] P. He, H. Wang, S. Liu, J. Shi, and M. Gong, *Appl. Phys. B: Lasers Opt.*, 99 (2010) 757-762.
[165] H. Yan, H. Wang, P. He, J. Shi, and M. Gong, *Inorg. Chem. Commun.*, 14 (2011) 1065-1068.
[166] H. Wang, P. He, S. Liu, J. Shi, and M. Gong, *Appl. Phys. B: Lasers Opt.*, 97 (2009) 481-487.
[167] L. Armelao, G. Bottaro, S. Quici, M. Cavazzini, C. Scalera, and G. Accorsi, *Dalton Trans.*, 40 (2011) 11530-11538.
[168] J. Wang, X. Jing, C. Yan, J. Lin, and F. Liao, *J. Lumin.*, 121 (2006) 57-61.
[169] F. Mo, L. Zhou, Q. Pang, F. Gong, and Z. Liang, *Ceram. Int.*, 38 (2012) 6289-6294.
[170] W.Q. Yang, H.G. Liu, G.K. Liu, Y. Lin, M. Gao, X.Y. Zhao, W.C. Zheng, Y. Chen, J. Xu, and L.Z. Li, *Acta Mater.*, 60 (2012) 5399-5407.
[171] C.-H. Chiu, M.-F. Wang, C.-S. Lee, and T.-M. Chen, *J. Solid State Chem.*, 180 (2007) 619-627.
[172] J.M. Postema, W.T. Fu, and D.J.W. IJdo, *J. Solid State Chem.*, 184 (2011) 2004-2008.
[173] W. Van Schaik and G. Blasse, *Chem. Mater.*, 4 (1992) 410-415.
[174] T. Saito, H. Sato, and T. Motegi, *J. Alloy. Compd.*, 425 (2006) 145-147.
[175] M.A. Rabah, *Waste Manage.*, 28 (2008) 318-325.
[176] F. Yang, F. Kubota, Y. Baba, N. Kamiya, and M. Goto, *J. Hazard. Mater.*, 254–255 (2013) 79-88.
[177] I. De Michelis, F. Ferella, E.F. Varelli, and F. Vegliò, *Waste Manage.*, 31 (2011) 2559-2568.
[178] K. Binnemans, P.T. Jones, B. Blanpain, T. Van Gerven, Y. Yang, A. Walton, and M. Buchert, *J. Clean. Prod.*, 51 (2013) 1-22.
[179] X.-F. Qiao and B. Yan, *Inorg. Chem.*, 48 (2009) 4714-4723.
[180] B. Francis, D.B.A. Raj, and M.L.P. Reddy, *Dalton Trans.*, 39 (2010) 8084-8092.
[181] S. Akerboom, W.T. Fu, M. Lutz, and E. Bouwman, *Inorg. Chim. Acta*, 387 (2012) 289-293.
[182] S. Akerboom, X. Liu, S.H.C. Askes, I. Mutikainen, W.T. Fu, and E. Bouwman, Submitted (2013).
[183] S. Akerboom, J.J.M.H. van den Elshout, I. Mutikainen, W.T. Fu, and E. Bouwman, *Polyhedron*, In press (2013).
[184] S. Akerboom, J.J.M.H. Van den Elshout, I. Mutikainen, M.A. Siegler, W.T. Fu, and E. Bouwman, *Eur. J. Inorg. Chem.*, Submitted (2013).
[185] S. Akerboom, M.S. Meijer, M.A. Siegler, W.T. Fu, and E. Bouwman, *J. Lumin.*, 145 (2014) 278-282.